Cardiac Microvascular Disease Quantified with CMR

Gyllenhammar, Tom

2021

Document Version:
Publisher's PDF, also known as Version of record

Cardiac Microvascular Disease Quantified with CMR

TOM GYLLENHAMMAR, M.D.
DEPARTMENT OF CLINICAL PHYSIOLOGY | FACULTY OF MEDICINE | LUND UNIVERSITY

Printed by Media-Tryck, Lund 2021 NORDIC SWAN ECOLABEL 3041 0903

TOM GYLLENHAMMAR was born December 8th, 1988, and grew up in Söderköping on the east coast of Sweden. He graduated from Lundsbergs boarding school in 2007 and earned his medical degree at Lund University in 2013. Outside work, he has a particular interest in mountain biking and always prioritizes spending time with his wife and daughters.

LUND UNIVERSITY

FACULTY OF MEDICINE

Department of Clinical Physiology

Lund University, Faculty of Medicine
Doctoral Dissertation Series 2021:79
ISBN 978-91-8021-085-0
ISSN 1652-8220

Cardiac Microvascular Disease Quantified with CMR

Cardiac Microvascular Disease Quantified with CMR

Tom Gyllenhammar, M.D.

LUND
UNIVERSITY

Thesis for the degree of Doctor of Philosophy

Thesis advisors: Prof. Håkan Arheden, M.D., Assoc. Prof. Marcus Carlsson, M.D., Prof. Henrik Engblom, M.D.

Faculty opponent: Prof. Jürg Schwitter, M.D.

To be presented, with the permission of the Faculty of Medicine at Lund University, for public criticism in the Segerfalk lecture Hall (Segerfalksalen) at BMC, Sölvegatan 17, Lund, Sweden on Friday, 17th of September 2021 at 14:00.

Organization LUND UNIVERSITY	Document name DOCTORAL DISSERTATION
	Date of issue 2021-09-17
	Sponsoring organization
Author(s) Tom Gyllenhammar	

Title and subtitle

Cardiac Microvascular Disease Quantified with CMR

Abstract

This thesis has investigated three different diagnoses where cardiac microvascular disease is suspected: hypertrophic cardiomyopathy (HCM), systemic sclerosis (SSc), and patients with suspected microvascular angina (MVA).

Study I of this thesis investigated patients with HCM. We investigated the myocardial perfusion (MP) using cardiac magnetic resonance imaging (CMR) in young patients with HCM or the risk of developing the disease. The investigation found that the patients had lower blood flow of the heart muscle than a reference group with healthy volunteers. This finding was interpreted as a sign of cardiac microvascular disease.

Study II investigated patients with SSc, which is a complex rheumatic disease with multiorgan involvement. The investigation showed that the patients had lower blood flow through the heart muscle than a reference group with healthy volunteers. This finding was interpreted as a sign of cardiac microvascular disease.

Study III Investigated patients with suspected MVA. The investigation showed that these patients had lower global MP than a reference group of healthy volunteers, but not as low as another reference group with patients with known coronary artery disease. The finding was interpreted as a sign of cardiac microvascular disease in this group of patients.

Study IV aimed to collect reference values for coronary sinus (CS) flow derived global MP and to validate the method against a flow phantom. The study showed that global MP was lower in men than women, which needs to be recognized when interpreting a quantitative assessment of global MP. The study also showed that the CS flow method is accurate compared to a flow phantom

Key words: cardiac microvascular disease, magnetic resonance imaging, microvascular dysfunction, hypertrophic cardiomyopathy, systemic sclerosis, microvascular angina.

Classification system and/or index termes (if any):

Supplementary bibliographical information:	Language English
ISSN and key title: 1652-8220	ISBN 978-91-8021-085-0
Recipient's notes	Number of pages 162 / Price
	Security classification

Cardiac Microvascular Disease Quantified with CMR

Tom Gyllenhammar, M.D.

LUND
UNIVERSITY

Cover: Photograph of a Hoya kerrii by Tom Gyllenhammar, retouched by Björn Dahlgren

Typeset in LaTeX

Faculty of Medicine, Department of Clinical Physiology
ISBN: 978-91-8021-085-0
ISSN: 1652-8220
Lund University, Faculty of Medicine Doctoral Dissertation Series 2021:79

Printed in Sweden by Media-Tryck, Lund University, Lund 2021

”One of the biggest things holding people back from doing great work is the fear of making something lame.” - Paul Graham

Contents

Papers

This thesis is based on the following publications and manuscripts:

I **Young patients with hypertrophic cardiomyopathy, but not subjects at risk, show decreased myocardial perfusion reserve quantified with CMR**

Tom Gyllenhammar, Eva Fernlund, Robert Jablonowski, Jonas Jögi, Henrik Engblom, Petru Liuba, Håkan Arheden, Marcus Carlsson

European Heart Journal - Cardiovascular Imaging. 2014 Dec;15(12):1350-7

II **Decreased global myocardial perfusion at adenosine stress as a potential new biomarker for microvascular disease in systemic sclerosis: A magnetic resonance study**

Tom Gyllenhammar, Mikael Kanski, Henrik Engblom, Dirk M Wuttge, Marcus Carlsson, Roger Hesselstrand, Håkan Arheden

BMC Cardiovascular Disorders. 2018 Jan 30;18(1):16

III **Myocardial perfusion assessed with CMR coronary sinus flow shows sex differences and lower perfusion in patients with suspected microvascular angina**

Tom Gyllenhammar, Marcus Carlsson, Jonas Jögi, Håkan Arheden, Henrik Engblom

Submitted manuscript.

IV **Age and sex-specific normal values of global myocardial perfusion from cardiac MR imaging of coronary sinus blood flow: Validation with a pulsatile flow phantom**

Tom Gyllenhammar, Henrik Engblom, Johannes Töger, Marcus Carlsson, Håkan Arheden

Manuscript.

Abbreviations

CAD coronary artery disease. 6–9, 21, 23, 40, 41, 45, 47

CFR coronary flow reserve. 7, 8, 11, 12, 41, 45

CMD coronary microvascular dysfunction. 7, 9, 11, 12, 37, 40, 41, 43, 45, 53

CS coronary sinus. 6, 7, 12, 13, 21, 23, 27, 30, 33, 38–40, 43, 48, 50, 54

EDV end-diastolic volume. 27

ESV end-systolic volume. 27

FA flip angle. 16

FFR fractional flow reserve. 9

FLAIR fluid attenuated inversion recovery. 17

GRE gradient-echo. 17, 32

HCM hypertrophic cardiomyopathy. 9, 10, 21, 23, 25, 37–40, 53

INOCA ischemia and no obstructive coronary artery disease. 45

IR inversion recovery. 17, 32

LAD left anterior descending artery. 1, 4, 8, 45

LCx left circumflex artery. 1, 4

LGE late gadolinium enhancement. 27, 32, 43

LM left main coronary artery. 1

LV left ventricular. 4, 6, 7, 10, 27, 30, 38, 39, 50, 53

MACE major adverse clinical event. 7, 45

MP myocardial perfusion. 6–8, 10–13, 21, 27, 30, 37, 38, 40, 41, 43, 45, 47, 48, 50, 53, 54

MPS myocardial perfusion single photon emission computed tomography. 12, 27, 41, 45, 47

MR magnetic resonance. 13, 14, 16, 17

MRI magnetic resonance imaging. 6–8, 10–14, 17, 21, 23, 27, 30, 32, 33, 37, 41, 45, 47, 48, 50, 53, 54

MVA microvascular angina. 9, 11, 12, 21, 23, 27, 45, 47, 53

PET positron emission tomography. 6–8, 10, 12, 45, 48

PSIR phase-sensitive inversion recovery. 32

RCA right coronary artery. 1, 4

RF radio frequency. 13, 16–18

SE spin echo. 17

SSc systemic sclerosis. 9, 11, 21, 41, 43, 53

SSFP steady-state free precession MRI. 27, 30

STIR short tau inversion recovery. 17

TE time to echo. 16, 17

TI time to inversion. 17

TR repetition time. 16, 17

TTE transthoracic echocardiography. 6, 8

Popular summary

The heart is located in the middle of the chest, between the lungs. This muscular organ contains a right and a left side, each with an atrium on top and a larger ventricle at the bottom. The right side of the heart pumps blood through the lungs, where the blood is oxygenated, and carbon dioxide is ventilated, and then back to the heart. The left side of the heart pumps blood from the lungs to the rest of the body, where the oxygen is used as an oxidizer in the energy-metabolism. More specifically, the oxygen is used to oxidize carbohydrates and fat to carbon dioxide.

The body of an average person requires 5 liters of blood each minute of blood at rest in order to survive. During exercise, this demand rises until the maximum limit of the person's heart pumping performance is reached. For an average individual, this limit is about twenty liters per minute. The heart muscle itself requires about 4-5% of the total circulated blood volume to sustain its oxygen needs.

The blood is supplied to the heart muscle tissue through coronary arteries on the surface of the heart. These relatively large blood vessels may be clogged in the event of coronary artery disease. If such a coronary artery is suddenly completely blocked, the person will experience a heart attack, which may cause severe chronic damage to the heart muscle or even death due to acute loss of the ability to pump blood through the body.

The large coronary arteries are connected to smaller arterial vessels closer to the muscular tissue that is the final destination for the oxygenated blood. These small vessels are called arterioles and capillaries. The arterioles regulate the amount of blood that the local downstream capillaries receive, and the capillaries are the smallest vessels where oxygen and carbon dioxide exchange occur. Pathological processes affecting these micro structures are called cardiac microvascular disease.

This thesis has used cardiac magnetic resonance imaging to investigate three different diagnoses where cardiac microvascular disease is suspected: hypertrophic cardiomyopathy, systemic sclerosis, and patients with suspected microvascular angina.

Study I of this thesis investigated patients with hypertrophic cardiomyopathy, which is a disease were the cardiac wall thickens, without another underlying condition that can explain the growth. The disease may cause fatal arrhythmia and is the most common cause of sudden death in young persons and athletes. We investigated the heart muscle's blood flow using magnetic resonance imaging in young patients with hypertrophic cardiomyopa-

thy or at the risk of developing the disease. The study found that the patients had lower blood flow of the heart muscle than a reference group with healthy volunteers. This finding was interpreted as a sign of cardiac microvascular disease.

Study II investigated patients with systemic sclerosis, which is a complex rheumatic disease with multiorgan involvement. The investigation showed that the patients had lower blood flow through the heart muscle than a reference group with healthy volunteers. This finding was interpreted as a sign of cardiac microvascular disease.

Study III Investigated patients with chest pain, signs of insufficient blood flow through the heart on exercise ECG and normal results when investigated with cardiac scintigraphy. These patients were classified as having suspected microvascular angina. The investigation showed that these patients had lower blood flow through the heart muscle than a reference group of healthy volunteers, but not as low as another reference group with patients with known coronary artery disease. The finding was interpreted as a sign of cardiac microvascular disease in this group of patients, that in today's clinical routine otherwise are relieved from suspicion of ischemic heart disease by cardiac scintigraphy.

Study IV aimed to collect reference values for one of the methods used in this thesis that is based on measurements of the blood flow through the cardiac muscle's large vein using magnetic resonance imaging. We also made control measurements against a computer controlled mechanical pump to characterize the precision of the magnetic resonance imaging method.

In conclusion, this thesis shows that:

I Patients with hypertrophic cardiomyopathy have lower blood flow through the cardiac muscle then healthy volunteers.

II Patients with systemic sclerosis have lower blood flow through the cardiac muscle than healthy volunteers.

III Patients with suspected microvascular angina have lower blood flow through the cardiac muscle than healthy volunteers.

IV We have compiled reference values for the blood flow through the cardiac muscle from healthy volunteers and also showed that coronary sinus flow derived global myocardial perfusion by magnetic resonance imaging is accurate compared to a flow phantom.

Populärvetenskaplig sammanfattning

Hjärtat är ett muskulärt organ lokaliserat centralt i bröstkorgen, bakom bröstbenet. Det består av en höger- och vänstersida. Den högra sidan pumpar blodet genom lungorna, där blodet syresätts och koldioxid vädras ut. Hjärtats vänstra sidan pumpar blodet vidare från lungorna till resten av kroppens alla vävnader. Väl framme i vävnaden avges syrgasen från blodet för att användas som oxidationsmedel i hjärtmuskelcellernas energimetabolism, där kolhydrater och fett förbränns till koldioxid.

En genomsnittlig person i vilotillstånd behöver ett blodflöde om c:a fem liter/minut för att överleva. Vid ansträngning ökar detta behov till dess den maximala gränsen för personens hjärtas pumpförmåga har uppnåtts, vilket är ungefär tjugo liter/minut. Hjärtmuskeln i sig kräver cirka fyra till fem procent av den totala blodvolymen för att tillgodose sitt eget behov av syrgas och energi.

Blodet levereras till hjärtmuskeln genom kranskärlen, som slingrar sig längs hjärtats utsida. Dessa relativt stora blodkärl kan, i händelse av så kallad kranskärlssjukdom, vara drabbade av förträngningar. Om ett kranskärl plötsligt blockeras drabbas personen av en hjärtinfarkt på grund av att hjärtmuskulaturen nedströms blockaden får akut syrebrist. En hjärtinfarkt kan orsaka allvarlig kronisk skada på hjärtmuskeln och i värsta fall leda till döden.

De stora kranskärlen är anslutna till mindre kärl, vilka benämns arterioler och kapillärer. Dessa små kärl ligger närmare hjärtmuskelvävnaden, som är slutmålet för det syresatta blodet. Arteriolerna har till uppgift att reglera mängden blod till kapillärerna, som befinner sig nedströms i den lokala muskelvävnaden. Dessa kapillärer är de allra minsta blodkärlen i systemet. I kapillärerna sker syrgas och koldioxidutbytet. Sjukdomsprocesser som drabbar dessa små blodkärl i hjärtat kallas mikrovaskulär hjärtsjukdom.

Denna avhandling har med magnetresonanstomografi (MR) undersökt tre olika sjukdomar där mikrovaskulär hjärtsjukdom misstänks föreligga: hypertrof kardiomyopati (HCM), systemisk skleros (SSc), samt patienter med bröstsmärta av misstänkt mikrovaskulär genes. Avhandlingen tillhandahåller även ett referensmaterial från friska personer för en av mätmetoderna.

Studie I i avhandlingen undersökte hjärtmuskelns blodförsörjning hos unga patienter med hypertrof kardiomyopati (HCM), samt personer med ärftlig risk att utveckla sjukdomen. HCM karaktäriseras av en sjuklig tillväxt av hjärtmuskeln och är den vanligaste

orsaken till plötslig död hos unga personer och idrottare. Den ökade dödligheten orsakas av allvarliga hjärtrytmrubbningar som kan leda till att hjärtat att sluta slå. Vår studie visade att patienter med HCM har ett lägre blodflöde i hjärtmuskeln jämfört med en referensgrupp med friska försökspersoner. Detta fynd tolkades som ett tecken till mikrovaskulär hjärtsjukdom i patientgruppen. Gruppen med personer med endast ärftlig risk att utveckla HCM visade ingen skillnad i blodförsörjning jämfört med friska försökspersoner.

Studie II undersökte patienter med systemisk skleros (SSc), som är en komplex reumatisk sjukdom med ofta multipelt organengagemang. Sjukdomen är förknippad med sjukliga förändringar i framför allt huden, men även i små blodkärl. Vår studie visade att patienter med SSc har ett lägre blodflöde genom hjärtmuskeln än en referensgrupp med friska försökspersoner. Detta resultat tolkades som ett tecken till mikrovaskulär hjärtsjukdom i patientgruppen.

Studie III undersökte patienter med bröstsmärtor och tecken på syrebrist i hjärtmuskeln vid arbets-EKG, men där hjärtscintigrafi inte kunnat påvisa några tecken på förträngningar i de stora kranskärlen. I vår studie undersöktes dessa patienter med MR och vi fann att patienterna hade lägre blodflöde genom hjärtmuskeln än en referensgrupp med friska försökspersoner. Fyndet tolkas som ett tecken på mikrovaskulär hjärtsjukdom även i denna patientgrupp.

Studie IV syftade till att samla in ett referensmaterial för en av de MR metoder som användes i denna avhandling. Denna metod utgår från mätningar med MR av blodflödet i hjärtmuskelns samlingsven. I studien genomfördes också kontrollmätningar med MR-kameran mot en datorstyrd mekanisk pump, för att undersöka MR-metodens mätprecision.

Resultaten av studien visade att metoden som användes vid mätning av sinus coronariusblodflödet har en god precision jämfört mot den mekaniska pumpen, men att sinus coronariusmetoden ger högre värden än PET och kvantitativ förstapassage perfusion med MR.

Nedan listas studiernas slutsatser i korthet:

I Patienter med hypertrof kardiomyopati har sämre blodförsörjning av hjärtmuskeln jämfört med friska försökspersoner.

II Patienter med systemisk skleros har sämre blodförsörjning av hjärtmuskeln jämfört med friska försökspersoner.

III Patienter med bröstsmärta av misstänkt mikrovaskulär genes har sämre blodförsörjning av hjärtmuskeln jämfört med friska försökspersoner.

IV Ett referensmaterial för hjärtats normala blodförsörjning från friska personer har sammanställts.

Acknowledgements

Without the contributions from many people, the work of this thesis would not have been accomplished. To you, I would like to send my deepest appreciation for the assistance you have provided me throughout the years that I have been working with this thesis.

First of all, I would like to thank my supervisor **Håkan Arheden** for introducing and guiding me through the world of scientific research. Besides that, I deeply appreciate the many conversations we've had about leadership and professionalism throughout the years.

My co-supervisor, **Marcus Carlsson**. Thank you for your immense support through all the work in the studies of this thesis. It has been very inspiring and developing to work with you.

My co-supervisor, **Henrik Engblom**. Thank you for all the great collaborations, support, and supervision throughout the projects and for always being encouraging.

Sebastian Bidhult, for always taking your time to explain physics and engineering, and for always sharing your great sense of humor. **Johannes Töger** for always being supportive, being an excellent collaborator, and for always helping out with any engineering challenge that may emerge. **Robert Jablonowski** for introducing me to the group and for great collaborations, especially with the first study of this thesis. **Jonas Liefke** for many interesting discussions and for giving constructive feedback on the thesis summary. **Ann-Helen Arvidsson** and **Christel Carlander** for great collaboration, especially for helping me to scan the patients in the different studies. **Einar Heiberg**, **Jane Tufvesson**, and **Helen Fransson** for many interesting discussions and delivering great software and support. **Roger Hesselstrand** for being a encouraging friend and collaborator. Without your support, this thesis would not have been accomplished.

To my colleagues in the Cardac MR Group, the Departement of Clinical Physiology and collaborators other departments for all support and collaborations, **David Nordlund**, **Anthony Aletras**, **Petter Friberg**, **Felicia Seemann**, **Pia Sjöberg**, **Katarina Steding Ehren-**

borg, **Mikael Kanski**, **Per Arvidsson**, **Eva Fernlund**, **Jonas Jögi**, **Dirk M. Wuttge**, **Ulrika Palm**, **Mariam Al-Mashat**, **Shahnaz Akil**, **Fredrik Hedeer** and **Anna Sakaria**.

To my friend **Torgil Bråberg** for helping me with feedback on the thesis summary and for helping me to construct figures for the Physics of the MR signal section. To **Richard Petterson** and **Mattias Haglund** - Thank you for helping me with constructive comments for my thesis summary and for being my friends through all the years as a research student.

To my beloved wife **Sara** and to my lovely daughters **Isabella**, **Patricia** and **Cornelia** for your great support and for accepting the many late nights I've spent working with my projects. To my parents **Ingvar** for marinating me in scientific curiosity and **Elisabeth** for sharing your experience of being a great teacher and learning me to put things in perspective. To my brothers **John** and **Carl** for leading the way through the many years in school and for always being encouraging.

Part I

Research context

Chapter 1

Introduction

1.1 The biology of myocardial perfusion

The heart is a muscular organ located in the center of the thorax. The heart contains a right and a left side. The right side pumps blood from the superior vena cava and inferior vena cava into the pulmonary circulation, where gas exchange of oxygen and carbon dioxide occurs. The left side of the heart pumps blood from the pulmonary veins into the aortic entry of the systemic circulation. The amount of blood that the heart pumps each minute is called the cardiac output.

The body of an average person requires 5 L/min of blood to remain in homeostasis at rest. During increasing exercise, this demand rises until the maximum limit of the person's cardiac output is reached. For an average person, this limit is about 20 L/min. The heart itself requires about 4-5% of the cardiac output at rest to sustain its energy and oxygen needs. The subsections below describe the blood's journey from the coronary arteries' entry through the myocardial capillaries, the coronary veins, and the final exit to the right atrium.

1.1.1 Coronary arteries

The epicardial coronary arteries are typically 0.5-5.0 mm in diameter. These vessels add very little vascular resistance to the coronary circulation under healthy circumstances. The vessel wall of these arteries consists of three layers: the outermost *adventitia* that contains nerves and a network of small blood vessels that supply the artery itself; the central *media* that contains smooth muscle cells; and the innermost *intima* that harbors the vascular endothelium that provides a barrier against the bloodstream, Figure 1.1.

There are two main branches of the coronary arteries, the left main coronary artery (LM) and the right coronary artery (RCA). The LM emerges from the root of the aorta next to the left cusp of the aortic valve. After about 1-2 cm, LM splits to form the left anterior descending artery (LAD) and the left circumflex artery (LCx). The gross anatomy of the coronary vessels is illustrated in Figure 1.2.

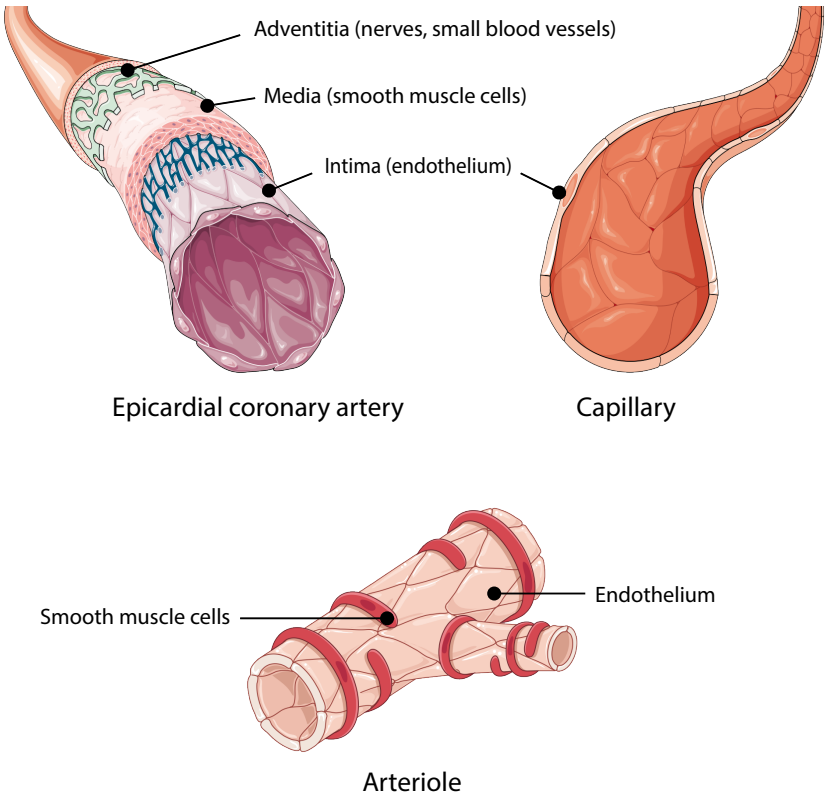

Figure 1.1: Histological overview of the epicardial coronary arteries, arterioles and capillaries constituting the arterial coronary circulation. The vessel walls of these arteries consists of three types of layers: the *adventitia* that contains nerves and a network of small blood vessels that supply the artery itself; the *media* that contains smooth muscle cells; and the *intima* that harbors the vascular endothelium that provides a barrier against the bloodstream. *Illustration by: Servier Medical Art, CC BY 3.0 <https://creativecommons.org/licenses/by/3.0>. Original illustrations arranged in a collage with added annotations.*

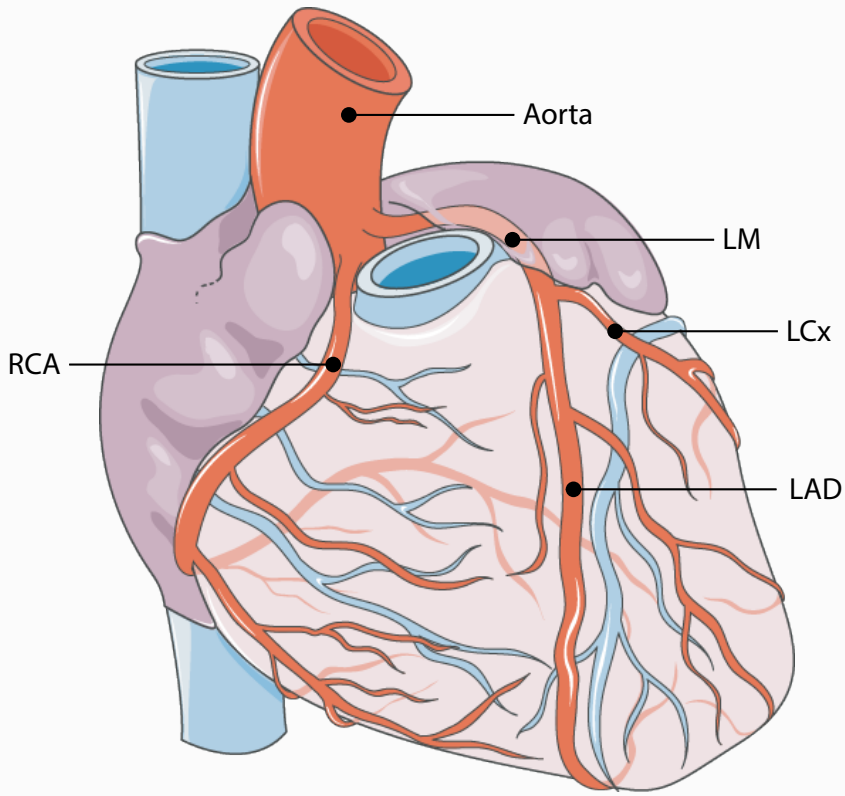

Figure 1.2: Anatomical overview of the epicardial coronary arteries. LM = Left main coronary artery, LAD = Left anterior descending artery, RCA = Right coronary artery, LCx = Left circumflex artery. *Illustration by: Servier Medical Art, CC BY 3.0 <https://creativecommons.org/licenses/by/3.0>. Annotations added to the original illustration.*

The LAD descends along the anterior interventricular sulcus and supplies the anterior wall and interventricular septum with blood. About half of the blood supply to the left ventricular (LV) myocardium comes from the LAD. Consequently, an occlusion of LAD, if left untreated, poses an acute risk of being fatal. The LCx follows the left coronary sulcus and supplies the posterolateral LV myocardium. From the LCx, one or more left marginal artery branches divert.

The RCA arises from the root of the aorta next to the right cusp of the aortic valve and descends along the right coronary sulcus. It supplies the right ventricle, right atrium and the posterior portion of the interventricular septum of the heart with blood.

The posterior descending artery supplies the inferior portion of the heart. This artery may either arise from the end of LCx, the end of RCA, or a combination of both.

Thinner, transmural branches that dives into the myocardium are emitted from the epicardial arteries. These transmural arteries compress during systole by the increased intramural pressure from the myocardial contraction, which is why little blood flow can perfuse the myocardium at this stage (Figure 1.3). Instead, the epicardial arteries elastically buffer the incoming blood-volume, which is passed down to the intramural vessels during diastole when the myocardium relaxes and the intramural pressure decreases.

1.1.2 Pre-arterioles, arterioles, and capillaries

The microvascular circulation of the myocardium includes the pre-arterioles, arterioles, and capillaries, Figure 1.1. The arteries connect to pre-arterioles ranging from 100-500μm in diameter. The key function of the pre-arterioles is to maintain a steady pressure for the arterioles. The pressure is regulated through local sensing of pressure and flow, and is not directly controlled by metabolic signaling from downstream myocytes.

The pre-arterioles branch to the arterioles, which are small vessels ranging 10-100μm in diameter. The main function of the arterioles is to regulate blood flow to the thinner capillaries that supply the myocytes. This regulation is conducted by a thin layer of smooth muscle cells that is able to change the arteriole diameter, hence changing vascular resistance. The call to the arteriole to adjust the blood flow is mainly sent from the myocytes downstream. Whenever the myocyte's intracellular oxygen level decreases, there is an increase of vasodilator signaling substances released to the local microenvironment. One of these potent vasodilator substances is adenosine. Adenosine levels are increased during oxygen depletion due to increased adenosine triphosphate degradation. Adenosine is released from the myocyte to the adjacent interstitial space, where it signals to the smooth muscle cells of the arterioles to dilate.

The arterioles connect to the smallest vessels of the system, the capillaries. The capillaries are about 5-8μm in diameter and consist of a single layer of endothelial cells. The role of the capillaries is to facilitate diffusion of blood gases, nutrients and metabolites between the blood and the interstitium surrounding the myocytes.

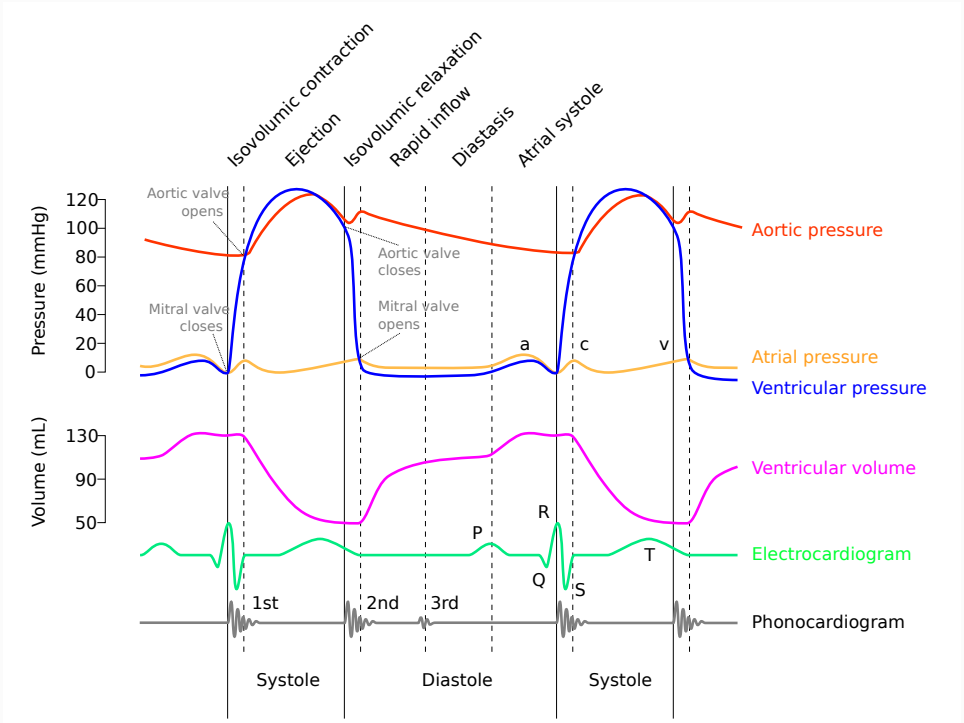

Figure 1.3: A Wiggers diagram[1] showing the events of the cardiac cycle. The perfusion of the myocardium takes place mainly during the ventricular relaxation (diastole). During the ventricular contraction (systole) the ventricular wall pressure is increased which reduces the myocardial perfusion. Red line = Aortic pressure, yellow line = atrial pressure, blue line = ventricular pressure, pink line = ventricular volume, green line = electrocardiogram (ECG), gray line = phonocardiogram annotated with the position of the heart tones. *Illustration by: adh30 revised work by DanielChangMD who revised original work of DestinyQx; Redrawn as SVG by xavax - Wikimedia Commons: Wiggers Diagram.svg, CC BY-SA 4.0, https://commons.wikimedia.org/w/index.php?curid=50317988*

1.1.3 Coronary veins

The deoxygenated blood flows from the capillaries to the venules and is returned downstream to the right atrium through the coronary veins. 95% of the LV drainage is collected through the great cardiac vein, middle cardiac vein, small cardiac vein, and LV posterior vein, which join to form the coronary sinus (CS) that exits into the right atrium[2]. The venous flow from the right chamber is collected by the anterior cardiac veins that individually connect and empty into the right atrium's anterior wall.

1.2 Methods to diagnose cardiac microvascular dysfunction

Due to spatial resolution limitations, no current non-invasive technique can directly visualize cardiac microvascular disease or dysfunction in vivo. Nevertheless, it is possible to indirectly detect unhealthy microvasculature by measuring the functional abilities of the microvascular system. Because functional tests cannot differentiate microvascular from epicardial coronary artery disease, the latter must be ruled out by preferably coronary angiography or possibly CT-angiography. If invasive measures are not available, microvascular disease should still be suspected if there is no regional hypoperfusion but pathological findings on functional imaging.

Several methods can be used to assess the functional abilities of the microvascular system, such as cardiac magnetic resonance imaging (MRI), cardiac positron emission tomography (PET), transthoracic echocardiography (TTE), and coronary angiography. A brief overview of these methods is given below, with extra focus on cardiac MRI given the scope of this thesis. The maximum blood velocity or blood flow during pharmacological stress, or the ratio between stress and rest is commonly used to describe the vasodilatory capacity of the coronary microvascular system. Adenosine, regadenoson, or dipyridamole which causes endothelium-independent vasodilation of the coronary circulation are widely utilized to test the functional properties of the vascular bed.

Adenosine is the vasodilator that has been used in the studies within this thesis and is known to increase the coronary blood flow up to for times by stimulating the adenosine A_2 receptor[3]. The sympathetic Beta 1-adrenoreceptor agonist dobutamine may also be used. Dobutamine causes an increase in cardiac workload, mimicking the effect of physical exercise. A third method to induce vasodilation is by performing a cold pressor test. A cold pressor test begins with submerging the patient's hand in ice-cold water. The pain will cause an increase in heart rate and blood pressure, which induces vasodilation of the pre-arterioles and thereby increasing the myocardial perfusion (MP)[4, 5].

Cardiac MRI

Cardiac MRI has the highest indication (class 1A 2014 ESC/EATS Guidelines on myocardial revascularization) for diagnostic testing of symptomatic patients with suspected stable coronary artery disease (CAD)[6]. Cardiac MRI can measure both regional and global

MP. Regional MP is measured using first-pass perfusion techniques, while global MP is calculated by either averaging all segments from quantitative first-pass perfusion, or by calculating the value from the CS flow and LV mass.

When data collection was conducted for the studies included in this thesis, fully quantitative first-pass perfusion was not available but has been developed since. The principle of first-pass perfusion is that a bolus of the paramagnetic gadolinium-based contrast agent is injected while SSFP images are continuously collected[7]. During the first pass of the contrast agent through the myocardium, there is an increase in the signal intensity of the myocardium proportional to the perfusion of the tissue. Differences in signal intensity between healthy myocardium (bright) and hypoperfused (black) myocardium can be recognized by visual inspection of the images[8]. The method has shown high diagnostic performance to detect significant CAD[9–11] and has similar diagnostic performance as cardiac PET[12].

Lately, a quantitative, dual sequence, single bolus first-pass perfusion method has been developed and is deployed in our research group[13, 14]. Using this method, measurements in low-resolution proton density images optimized for high gadolinium concentration in the LV blood pool are used to calculate the arterial input function. In addition, high-resolution perfusion images are acquired. Motion correction and conversion of signal intensities to gadolinium concentration are performed, and quantitative perfusion maps of the LV are constructed. More importantly, quantitative first-pass perfusion has shown improved diagnostic strength over visual analysis to detect significant obstructive CAD[15] and to detect coronary microvascular dysfunction in in patients with angina and nonobstructive coronary artery disease[16].

An alternative approach used to quantify global MP with cardiac MRI is to measure the ratio between the blood flow in the CS and the LV mass at stress and rest. The CS flow method is well-validated phantom experiments and in-vivo and benefits from being independent of models that adjust for non-linearities between signal and contrast media as in the case with quantitative first-pass perfusion[17–22]. Combining the information from global MP with that of the first-pass perfusion increases the ability to localize patients with significant CAD, and the SYNTAX score is higher in patients with low coronary flow reserve (CFR) from CS global MP as a sign of multivessel disease[23]. Using a combination of catherization during exercise and adenosine stress cardiac MRI, patients with angina without obstructive CAD and a CFR < 2.5 has been shown to have both a disrupted physiological response to exercise and global myocardial ischemia, contrary to patients with normal coronary flow reserve[24].

Even in the absence of fibrosis or regional hypoperfusion, CFR from MRI CS flow measurements has been shown to be an independent predictor of major adverse clinical event (MACE) in patients with known or suspected coronary artery disease, which further strengthens the argument for using CFR from MRI CS flow measurements to detect coronary microvascular dysfunction (CMD)[25].

A more in-depth description of the MRI technology is given under the section "Magnetic resonance imaging".

Cardiac PET

Cardiac PET is an established method for non-invasive measurements of MP. Like cardiac MRI, cardiac PET also has the highest indication (class 1A 2014 ESC/EATS Guidelines on myocardial revascularization) for diagnostic testing of symptomatic patients with suspected stable CAD[6]. The method is based on measurements of radiated photons from a radioactive tracer that has been injected intravenously in the patient[26, 27]. There are many radioactive tracers that can be used when performing a cardiac PET, such as Rubidium-82, Nitrogen-13 ammonia, and Oxygen-15 water[28]. As the injected isotope undergoes positron emission decay, the emitted positron interacts with nearby electrons, causing the radiation of a gamma photon that is detected by the scanner. The number of detected photons is then used to calculate the perfusion from the tissue of interest. For instance, global MP by Nitrogen-13 ammonia PET has been validated with an excellent agreement ($r = 0.95$ to 0.96) against microspheres in canines experimentally[29].

Cardiac CT

CT can be used both to detect calcifications in the epicardial coronary arteries but also for functional imaging of the MP. Time-attenuation curves during the first pass of an iodine contrast medium are used to quantify the myocardial perfusion[30], and the method's ability to detect segments with hypoperfusion is validated against MRI[31]. The clinical application for functional imaging with CT is limited by the usage of high radiation doses and the need for a long breath-hold during the scan[31]. The method is also constrained by the technical requirement to reduce the heart rate during the examinations by the use of beta-blockers, which attenuates the effect of the vasodilators[32].

Echocardiography

Pulse-wave echocardiography can measure coronary blood flow velocity in the epicardial coronary arteries[33]. For TTE, the proximal LAD is usually examined due to its advantageous anatomical position, and the method has proved accurate compared to invasive measurements[34]. The measurements can be done in both rest and during pharmacological vasodilation, enabling calculations of CFR. CFR measurements in LAD by TTE have shown a good ability to predict the outcome in patients with suspected or known CAD using a dipyridamole stress/rest protocol where a CFR > 2 marks a significantly increased risk of poor outcome[35].

Invasive coronary angiography

Invasive coronary angiography is based on the injection of a radio-opaque contrast agent into the epicardial coronary arteries while visualizing the passage of the contrast using X-ray. Coronary blood flow velocity can be measured using a Doppler wire inserted in an epicardial coronary vessel[36], and blood flow can be estimated from the average velocity of the passing blood and the measured vessel diameter from the X-ray[37]. A coronary blood flow velocity reserve < 2.5 after percutaneous coronary intervention due to ST-elevation acute myocardial infarction was associated with a fourfold increased risk of long-term cardiac mortality, highlighting the clinical importance of a diseased microvasculature[38].

Stenotic lesions of epicardial coronary arteries can also be investigated with fractional flow reserve (FFR). FFR is a measure of the blood pressure drop across a stenosis in the epicardial coronary vessel and is used to describe the severity of the stenosis. Interestingly, CAD patients with a normal FFR but with an abnormal coronary flow velocity reserve have an increased risk for major adverse cardiac events rate throughout ten years of follow-up, independent of the FFR. In contrast, an abnormal FFR with a normal coronary flow velocity reserve shows a similar clinical outcome compared to patients with both normal FFR and coronary flow velocity reserve[39]. Though invasive coronary angiography enables a definite rule out of coronary artery stenosis in patients, the method is limited by its invasive nature. Hence, non-invasive functional imaging is recommended in patients with suspected stable CAD as the first line of diagnostics before deciding if proceeding with coronary angiography is necessary[6].

1.3 Diseases with coronary microvascular dysfunction

As described in the previous section about pre-arterioles, arterioles, and capillaries, there are many mechanisms involved in myocardial blood flow regulation, and these structures may be affected by cardiac microvascular disease. Pathological changes of the microvascular system that affect the normal regulation of the myocardial bloodflow is called cardiac microvascular disease (CMD). Such issues are seen in many diseases and commonly involves a combination of pathological alterations of the cardiac microvascular circulation. Contributing components may be endothelial dysfunction, smooth vascular cell dysfunction, vascular remodeling, increased intramural pressure, and luminal obstruction[40]. This thesis focuses on three different diseases with suspicion of CMD: hypertrophic cardiomyopathy (HCM), systemic sclerosis (SSc), and patients with suspected microvascular angina (MVA).

1.3.1 Hypertrophic cardiomyopathy (HCM)

The first disease investigated in this thesis is HCM. HCM is a disease where the myocardial wall thickness increases intrinsically and not due to an underlying condition, such as another cardiac, systemic, or metabolic disease[41].

The prevalence of persons with HCM phenotype, defined as a maximal LV wall thickness ≥ 15 mm and a non-dilated left ventricle, is about 0.2% in the general population[42, 43]. If also including persons carrying an HCM mutation, the prevalence is about 0.5%[44].

In about 6/10 HCM-patients, there is an autosomal dominant mutation of genes encoding sarcomere proteins[45, 46]. The sarcomeres are long proteins that slide past each other to contract the muscle fiber and create force. In about 1/10 of the HCM-patients, the disease is associated with other genetic disorders, syndromes, and chromosome disorders, and in the final 3/10 patients, the cause of hypertrophy is unknown[41].

Patients with a sarcomere protein mutation have a higher risk of progressive heart failure and death than patients who do not have such a mutation[47]. The highest risk of sudden cardiac death in patients with HCM is at the age of 9-12 years, with the most common cause being arrhythmia[48]. Furthermore, the disease is the most common cause of sudden death in young persons and athletes[49].

Out of the patients with a known mutation, the most common of these mutations, prevalent in 42%[50] of HCM-patients, is that of MYBPC3, which encodes the protein named Myosin Binding Protein. In knock-out mice, the function of Myosin Binding Protein is to inhibit the actin-myosin interaction, which acts as a brake on the muscle fiber shortening, reducing the overall exerted force on the tissue[51], and absence of the protein causes severe hypertrophy, myocyte disorganization, and interstitial fibrosis[52]. The second most common mutation is prevalent in 40%[50] of HCM-patients and is that of MYH7, which encodes the protein named Myosin Heavy Chain Beta. Myosin Heavy Chain Beta is a vital component of myosin and therefore plays a major role in myocyte contractility. The third most common mutation, prevalent in 6.5%[50] of HCM-patients, is in the TNNT2 gene which encode the protein named Cardiac Muscle Troponin T. This protein regulates myocyte contraction in response to changes in intracellular calcium ion concentration.

Ex vivo, pathological variations of the intramural coronary arteries have been observed in HCM. About 4/5 HCM-patients are found to have wall thickening of these vessels due to the proliferation of medial or intimal vessel components[53]. Moreover, a blunted increase of MP after administration of dipyridamole in studies using PET suggests microvascular dysfunction in the majority of the HCM-patients[54, 55]. Such an inadequate response to dipyridamole has proved to be strongly correlated to increased risk of heart failure progression and death[56]. In about 1/3 of the HCM-patients, severe microvascular dysfunction has been detected using MRI quantitative first-pass perfusion[57]. In these patients, areas with severe microvascular dysfunction not only failed to increase during adenosine stress, but decreased compared to the resting value[57].

When this thesis was planned, there was no previous study investigating the MP with MRI in young patients with HCM or risk of developing the disease. Study I in this thesis describes our work investigating the MP in these patients.

1.3.2 Systemic sclerosis (SSc)

The second disease investigated in this thesis is SSc, which is a rheumatic connective tissue disease with multi-organ involvement. The disease is characterized by collagen deposits in the skin, lungs, arteries, kidneys, heart, gastrointestinal tract, and muscles. The disease is associated with increased morbidity and mortality, and attempts to treat the disease need to be carefully tailored to fit the organ involvement of the individual patient[58].

SSc has a low prevalence of about twenty cases per one million and is more common in women than men[59]. The disease is divided into two major subgroups: the limited cutaneous form with skin involvement below the elbows and knees, but no proximal or facial involvement, and the diffuse cutaneous form with the additional engagement of the proximal extremities and the face[60].

The etiology of SSc is highly complex, with pathological changes currently known in three types of cells: fibroblasts, endothelial cells, and immune cells[61]. Changes in these cells often result in severe and progressive fibrosis of the skin and internal organs, such as a reduced lumen size of small arteries and arterioles, production of auto-antibodies, and mononuclear cell infiltration of affected tissues[61].

Patients with SSc also suffer from an increased risk of cardiovascular mortality[62] and have an increased prevalence of coronary atherosclerosis when compared to healthy controls[63]. The atherosclerosis occurs in both arterioles, small-, and medium-sized coronary arteries[63, 64] and an impaired CFR in SSc-patients was demonstrated already in 1985[65]. It has been hypothesized that repeated focal ischemia is the cause of the high prevalence of myocardial fibrosis in SSc-patients[66].

When this thesis was planned, there was limited knowledge about the MP in SSc-patients. Such knowledge could potentially be used to better understand the disease and inform development of new investigative methods and treatments. Therefore, study II of this thesis was designed to investigate the prevalence of CMD in SSc-patients by investigating their global MP with cardiac MRI.

1.3.3 Microvascular angina (MVA)

The third disease investigated in this thesis is MVA. Symptoms of significant epicardial coronary artery stenosis, such as chest pain or shortness of breath during exercise, are commonly examined by coronary angiography or non-invasive imaging of MP to rule out significant coronary artery stenosis. Despite no evidence of epicardial coronary stenosis on invasive angiography, up to 70% of patients with suspected ischemic chest pain show evidence of ischemia[67]. These patients are considered to suffer from MVA[68]. Although MVA-patients do not have epicardial coronary artery stenosis, they suffer from a worse prognosis than persons with normal findings on stress/rest perfusion imaging[69, 70].

Three different causes of MVA have been suggested[71]: 1) underestimation of the functional significance of coronary arterial stenosis on invasive angiography; 2) CMD; and 3) coronary spasm. Histological analysis has revealed obliteration of the arteriolar lumen

and decreased capillary density in heart-transplanted patients without epicardial coronary artery stenosis[72]. These findings indicate that microvascular disease may be present without coincident disease in the large coronary arteries and that the observed microvascular remodeling correlates with impaired microvascular function[72].

Patients with MVA have a worse prognosis than patients without myocardial ischemia[73]. Hypertension and diabetes have been recognized as risk factors for developing MVA[74–76]. However, independent of other risk factors, MVA detected by a decreased coronary flow reserve is an independent predictor of major adverse clinical advents. Furthermore, the issue with MVA has been highlighted as a source of undiagnosed chest pain, especially in women[77].

Currently, treatments for MVA are limited but a recently published abstract by Bowe et al. suggests that weight loss, increased physical activity, and optimized medical treatment for hypertension, dyslipidemia and diabetes reduce chest pain in patients with CMD[78]. However, despite the reduction of chest pain, Bowe et al. reported no increase in coronary flow velocity reserve[78].

Studies using PET or myocardial perfusion single photon emission computed tomography (MPS) have shown that patients with a very low coronary flow reserve (< 1.5) but without regional ischemia have a severely increased annual risk of death compared to healthy volunteers (3.6% vs. 0.1%)[79]. A threefold risk of major cardiovascular events has been observed for patients referred to MPS due to suspicion of ischemic heart disease[80].

At the time this thesis was planned, there were studies that had investigated CMD in patients with MVA, but there was no published work on CS flow derived global MP in such patients. Furthermore, there was limited knowledge about potential gender differences within the disease. Because of that, these matters were investigated in paper III of this thesis.

1.3.4 Reference values for CS flow derived global myocardial perfusion (MP)

The previous sections of this thesis describes diseases where cardiac microvascular disease may be suspected. Cardiac microvascular disease may cause CMD which may be detected by a reduction of global MP or CFR during a pharmacological stress/rest test. Currently, there are three candidates for non-invasive quantitative measurement of MP: 1) cardiac PET[26, 27]; 2) CS flow derived global MP[20]; and 3) MRI first-pass perfusion imaging[7, 14] and all three methods have successfully been used to investigate suspected CMD[81–83].

For CS flow derived global MP, however, there is a lack of gender-specific reference values from healthy persons that cover a clinically acceptable age range. Such reference values for CS flow derived global MP are needed to improve the usability of the method for future studies investigating CMD in diseases with suspected cardiac microvascular involvement.

Therefore, study IV of this thesis aimed to collect a reference data set on CS flow derived global MP from both young and old healthy men and women. The study also aimed to

validate MRI sequence used for the CS flow derived global MP method against a pulsatile flow phantom.

1.4 Magnetic resonance imaging

1.4.1 Historical background

The history of today's high-quality MRI dates back to the late 1930s when Isidor Isac Rabi conducted experiments demonstrating that electromagnetic radiation is emitted when molecules are sent through a magnetic field[84]. This phenomenon was named nuclear magnetic resonance (MR). Rabi also showed that the radio frequency (RF) of the emitted electromagnetic radiation is coupled to the type of molecule sent through the magnetic field. Further work was conducted by Felix Bloch and Edward Mills, who investigated the nuclear MR properties of solid materials and liquids. For these groundbreaking efforts, Rabi was awarded the 1944 Nobel prize in Physics, and Bloch and Mills the 1952 Nobel Prize in Physics[84, 85].

The concept the MR body scanner was proposed in 1969 by Raymond Damadian who also reported that tumour cells could be differentiated from normal cells using MR[86]. In the early 1970s, Paul Launterbur introduced methods describing how MR measurements could be transcoded into imagery[87]. Significant technological improvements were made by Peter Mansfield, who introduced frequency and phase encoding by spatial gradients of the magnetic field, which improved the speed and accuracy of the image acquisition[88]. The important work made by Lauterbur and Mansfield jointly awarded them the 2003 Nobel Prize in Physiology or Medicine.

In 1977 the first human body part (the intermediate phalanx in the middle finger of the right hand) was imaged using MR[89], and full-body images were finally achieved in august 1980[90]. In 1981 the first superconducting magnet was utilized in an MRI scanner[91]. From that time, the magnetic field strength has increased and 1.5-3T magnets are now common in clinical use. Large magnets with extreme field strengths of up to 10.5T and magnet weights of as much as 110 metric tons are used for research purposes[92].

Cardiac implementations of nuclear MR dates back to 1976 when energy metabolism in isolated rat hearts was investigated with phosphorus-31 nuclear MR spectroscopy[93]. Successful contrast imaging of myocardial infarction in canine models using paramagnetic ionic contrast agents was presented in 1982[94], and cardiac MRI of acute myocardial infarction in canine models recognizing alterations in T1 and T2 relaxation times was presented in 1983[95].

Myocardial perfusion imaging was introduced in 1990 using a bolus injection of gadolinium contrast agent with subsequent measurements of first-pass wash-in and wash-out of the contrast agent[96]. From that, the first pass perfusion technology has seen constant refinement, and it is now possible to extract fully quantitative myocardial perfusion maps at both rest and pharmacological stress testing in a clinical setting[13].

The concept of cardiovascular blood flow imaging was introduced in 1984 with sequence development, phantom experiments, and *in vivo* measurements of two volunteers' carotid and femoral arteries[97]. The technology behind flow measurements has also been subject to impressive development and it is now possible to acquire time resolved three-dimensional flow measurements in patients.

To summarize this section about MR history, the now available MRI technology is a translational research product spanning over almost a century. The benefit that it has brought to patient care cannot be overemphasized.

1.4.2 Physics of the MR signal

This section briefly describes the physics in MRI technology. Atoms contain a nucleus with positively charged protons, neutrally charged neutrons, and negatively charged electrons bound to the nucleus. The positively charged nucleus spins around its own axis. The movement of an electrical charge induces a magnetic field. Because of that, each nucleus is a tiny magnetic dipole with its magnetic vector pointing in the direction of the rotational axis of the nucleus. The human body contains about 60% water with the benefit that there are large amounts of hydrogen atoms whose magnetic properties are readily available for MR experiments.

When not subjected to an external magnetic field, the hydrogen atoms that make up the human body directs their magnetic vectors randomly in space. The sum of all these tiny magnets can be added together and described as the summed magnetic field M. When the body is outside the strong magnetic field of the MRI scanner, the net magnetization M is zero, and consequently, the magnetic field M has no direction. However, when the body is placed inside the strong magnetic field of the MRI scanner, B_0, the magnetic vectors of the individual hydrogen atoms are effected by B_0 and start to wobble, precessing around the directional axis of the magnetic field B_0. When the previously randomly spinning hydrogen atoms precess around the axis of the magnetic field B_0, the magnitude of M grows in the direction of B_0.

The frequency at which the hydrogen nucleus precess is called the Larmor frequency f_0 and is calculated as the field strength of $B_0 \times \gamma$. In this thesis, 1.5 T MRI scanners have been used, which operates at a frequency of approx. 64 MHz (1.5 T $\times$ 42.6 MHz/T). This is within the VHF-frequency band commonly used in many other radio technologies. To shield the system from external electromagnetic noise, the room that encloses the MRI scanner is carefully shielded with a Faraday cage.

To be able to extract information about M, it has to be separated from B_0. To do this, the direction of B_0 is used to construct a coordinate system, X, Y, and Z. As shown in Figure 1.4.A, Z is defined as the direction of the magnetic field of B_0, and X and Y are perpendicular to Z. M is then referenced relative to this coordinate system as the vector $\overrightarrow{M}$. By forcing the direction of $\overrightarrow{M}$ from its resting orientation parallel to Z, the properties of M are separated from B_0, and can be measured.

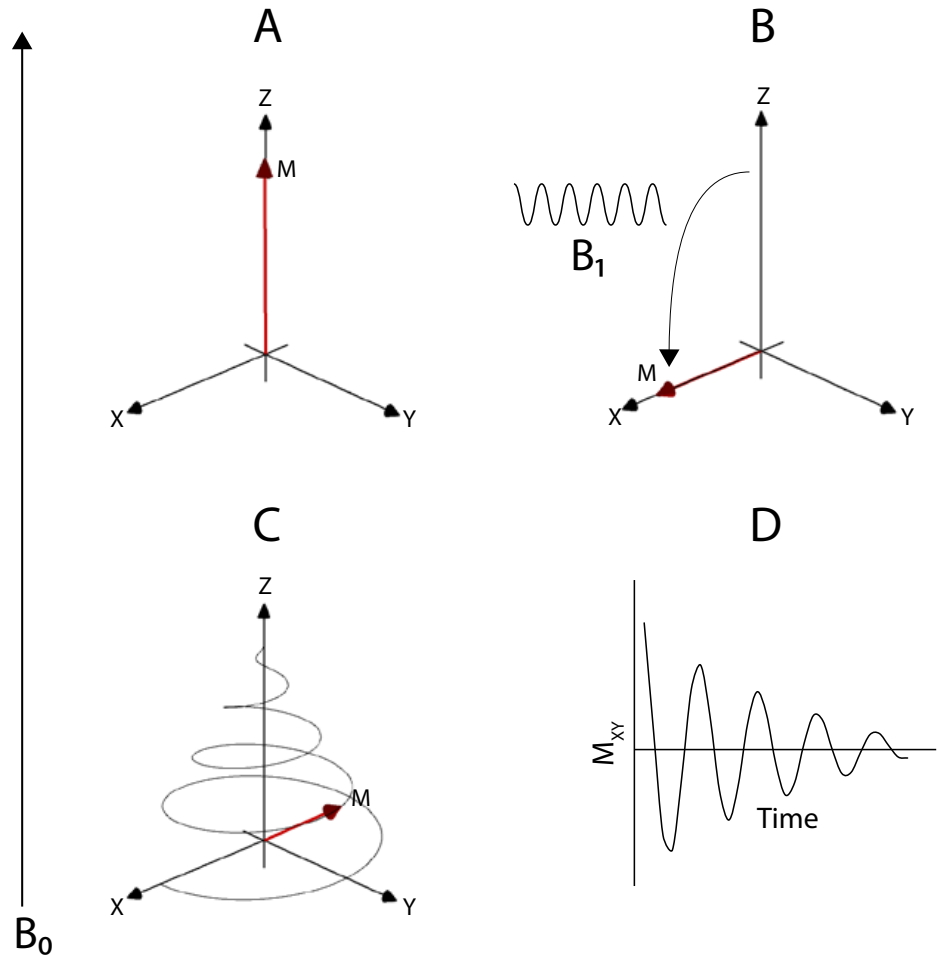

Figure 1.4: Illustration of how the MR signal is generated. The Z axis of the coordinate system is defined by the direction of the static magnetic field B_0 of the MRI scanner, while X and Y are perpendicular to Z. A: When the body is placed in B_0, the rotation of the summed magnetic vector M of the body's hydrogen nuclei align with the Z axis. B: A radio pulse B_1, in this example with a flip angle of 90°, is transmitted which causes M to precess perpendicular to the Z axis on the XY plane. C: When B_1 is turned off, the direction of M relaxes to Z in a spiral motion. D: The oscillation of the magnetic vector M in the XY plane induces a radio signal called free induction decay. This is the signal picked up by the radio receivers of the MRI scanner.

Deviation of $\overrightarrow{M}$ is induced by exposing the body inside the camera to an orthogonal oscillating electromagnetic field B_1 tuned to f_0. When exposed to B_1, the $\overrightarrow{M}$ reacts with a diversion of the precession axis of $\overrightarrow{M}$ as shown in Figure 1.4.B. The angle from the Z axis at which $\overrightarrow{M}$ precess is called the flip angle, α. The word "resonance" in "magnetic resonance imaging" refers to this phenomenon, where the radio wave resonate with the nuclei spins.

T1, T2, and T2*

When B_1 is turned off, $\overrightarrow{M}$ will return to its relaxed state in a complex pattern shown in Figure 1.4.C. The individual components of X, Y, and Z for $\overrightarrow{M}$ are used to describe the MR-signal in closer detail. The time it takes for 63% of $\overrightarrow{M}_Z$ to rebuild during relaxation after a 90° B_1 RF pulse is called T_1, and the time it takes for 63% the $\overrightarrow{M}_{XY}$ to dephase is called T_2.

The rebuild of $\overrightarrow{M}_Z$ and dephasing of $\overrightarrow{M}_{XY}$ are independent processes which is why T_1 and T_2 have different values for any given tissue.

T_1 is dependent on the microenvironment around the nuclei, such as surrounding molecules, temperature, and contrast media. For this reason, the $\overrightarrow{M}_Z$-relaxation is also called spin-lattice relaxation, with "lattice" referring to the surrounding microenvironment.

T_2 is, additional to effects of the microenvironment around the nuclei, also dependent on interactions with other proximate nuclei's magnetic fields. For this reason, T_2-relaxation is also called spin-spin relaxation.

In addition to T_1 and T_2 relaxation, there is also a dephasing of spins due to the magnetic field's inherent local inhomogeneity. These field strength variations cause the nuclei to precess at slightly different frequencies in the transversal XY plane during relaxation after a 90° RF pulse. The sum of transversal signal decay due to spin-spin interactions and local magnetic field inhomogeneity is called T_2*.

1.4.3 MRI parameters and sequences

There are many types of RF pulse sequences and parameters, each engineered to induce as much signal in return as possible for the specific type of tissue that is desired to be imaged. The paragraphs below discuss some of the basic parameters and pulse sequences that have been used in the different studies of this thesis.

Flip angle (FA) is the angle to which the spin is excited by the RF pulses. By lowering the FA, the time it takes for $\overrightarrow{M}_Z$ to rebuild is reduced. This is why the repetition time (TR) (described later) can also be reduced when FA is decreased without risking any unwanted attenuating effects. However, a flatter FA comes with the cost of a lower signal in the XY plane.

Time to echo (TE), is the length of the period from that an RF pulse is emitted until there is a peak in the returned signal, called an echo.

Inversion recovery (**IR**) RF pulses consist of a 180° pulse that flips $\overrightarrow{M}_Z$ to the negative $\overrightarrow{M}_Z$ axis. After a recovery period, referred to as **time to inversion** (**TI**), a second 90° RF pulse is transmitted, and signal readout is performed directly after the second pulse. IR pulse sequences are often used to collect T_1 weighted images. The length of TI is dialed to suppress the signals from unwanted tissue. For instance, the signals from fat are suppressed with short tau inversion recovery (STIR) sequences, and the signals from water are suppressed with fluid attenuated inversion recovery (FLAIR) sequences.

Spin echo (**SE**) RF pulses begin with a 90° excitation pulse that flips $\overrightarrow{M}$ to the XY plane. Due to local variations in the magnetic field, the RF varies slightly, causing a desynchronization of the magnetic movements, hence a decay of potential signal, on the XY plane. To overcome this, a second 180° refocusing pulse which flips the magnetic movements is transmitted. This has the effect that the individual magnetic movements reverses on the XY plane and begin to catch up. When synchronization of the individual magnetic movements occurs, a signal echo is detected.

The time interval between the first 90° excitation pulse and the second 180° refocusing pulse is referenced as τ. TE = 2τ which is why TE can be tuned by selecting an appropriate τ. Tuning TE is necessary since T_2 relaxation occurs as usual while waiting for the echo; hence the length of TE defines which type of tissue will dominate the signal in the echo.

Gradient-echo (**GRE**) sequences have similarities to the SE sequences. Just as with SE sequences, GRE sequences begin with a excitation pulse that flips $\overrightarrow{M}$ to the XY plane. The key difference is that re-phasing is accomplished with a magnetic gradient instead of a second refocusing RF pulse. Directly after the excitation RF pulse, a negative magnetic field gradient is applied. This causes the spins to precess at different frequencies depending on their positions in the now purposely inhomogeneous magnetic field. After a short period, an inverse positive magnetic field gradient is applied. This reverses the process, and after TE, a so-called GRE can be detected when the spins re-phase.

TR is the time between each consecutive repetition of a sequence. If the TR is shorter than the time it takes for $\overrightarrow{M}_Z$ to rebuild during relaxation completely, $\overrightarrow{M}$ will not be aligned with the Z axis when the next RF pulse is transmitted. This causes the returned signal to gradually decrease for each sequence in the train of repeated sequences. Since different tissues have different T_1 values, adjustment of TR can attenuate signals from specific tissues, increasing the contrast between attenuated and non-attenuated tissue in the final image.

1.4.4 Spatial encoding with gradient coils

In the previous sections, the fundamental principles of how to create an MR signal have been described. However, additional steps to spatially encode the signal to a specific position within the scanned tissue are needed. The signal's spatial encoding is done by specific hardware called magnetic gradient coils, and RF pulses purposed for spatial encoding.

Inside the MRI scanner's core, there are three electromagnets called gradient coils, which can be rapidly turned on or off by the machine. The gradient coils are designed

so that when a specific gradient coil is turned on, it induces an additional magnetic field in either the X, Y, or Z direction where Z is constrained to the direction of the static magnetic field, B_0. The gradient coils are designed to create magnetic gradients in the otherwise homogeneous B_0. For each of the three dimensions, the gradients are utilized differently and described in more detail below.

Z axis (slice selection)

The first step is to make a slice selection, in which signals only are collected from one position along the investigated tissue's Z axis. In other words, this is a method to get signals from only one cross-sectional slab of the body. By applying a magnetic gradient in the direction of the Z axis, the nuclear precession frequency will vary along the axis. By matching the RF pulse frequency to the specific precession rate for a given position along the Z axis, only nuclei located in that specific position will get excited. Because of this, only nuclei in the specific, selected slice will contribute to the read-out signal at the later stage; hence, the Z dimension has been encoded.

X axis (frequency encoding)

The second step is to encode the signal on the X axis in the remaining XY plane. This is done similarly to slice selection, but the difference is that the magnetic gradient is applied during signal readout instead of during excitation. By applying the gradient during signal readout, the nuclei in a specific position on the X axis will emit an RF signal with a frequency specific to the known magnetic field strength in that location. By that, the signal has been successfully encoded on the X axis.

Y axis (phase encoding)

The third and last step is to encode the remaining Y dimension. This is done by applying a magnetic gradient along the Y axis for a short period. During this period, the spins will precess at different rates along the Y axis, which causes them to precess asynchronously. This asynchrony is preserved when the magnetic gradient is switched off, and the nuclei return to precess at the same rate. The signal during readout will then contain the summed signal from the nuclei spinning at different phases. It is impossible to determine the proportion of the signal attributed to a specific phase with only one experiment. This is solved by rapidly repeating the experiment with increments in phase shift before each readout. By comparing the amplitude of the composed signal from the array of repeated experiments, it is possible to calculate the individual signal components originating from the different positions along the Y axis.

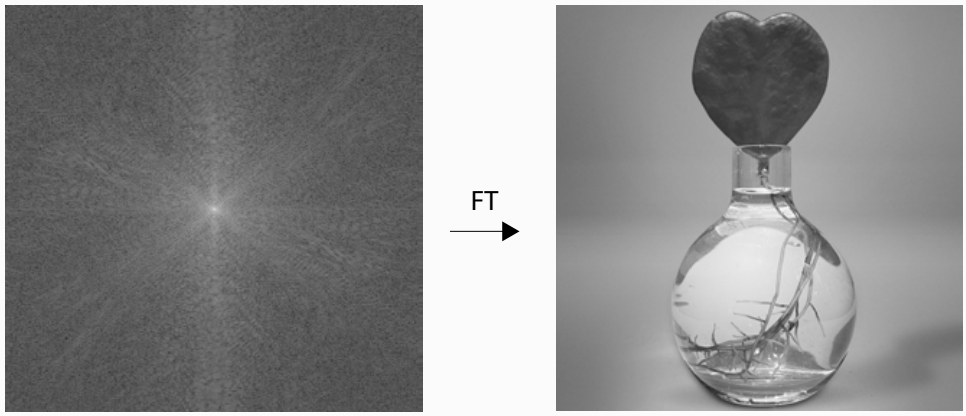

Figure 1.5: Illustration of image information arranged in k-space to the left and after a Fourier transform (FT) to the right. The positions in the k-space do not correspond to the positions of the pixels in the final image. Instead, each position in the k-space contains information about all pixels in the final image. k-space is equivalent to a diffraction pattern of the final image, and is translated by the Fourier transformation to a readable image.

1.4.5 k-space and Fourier Transformation

The radio signal registered during readout contains a mix of different frequencies with different amplitudes. The individual wave components are organized in a 2D matrix called k-space with the axes k_x, k_y. "k" stands for spatial frequency, defined as 1/wavelength. In other words, k is the number of wave tops by one length unit. Each step of the frequency encoding represents a column in k-space, and each step of the phase encoding represents a row. These positions are filled with the signal collected by the radio receivers during readout. The spatial positions in the k-space do not correspond to the pixel's spatial positions in the final image. Instead, each position in the k-space contains information about all pixels in the final image. k-space is equivalent to a diffraction pattern of the final image, which is why a Fourier transformation is needed to reveal the final readable image (Figure 1.5.

Chapter 2

Aims

Cardiac microvascular disease contributes to poor outcomes and suffering. Today, there are virtually no clinically available non-invasive diagnostic methods for cardiac microvascular disease. The development and refinement of such methods are needed for both improved diagnostics and the long-term goal of enabling treatments.

Therefore, the overall aim of this thesis is to determine how magnetic resonance imaging (MRI) can be utilized to determine myocardial perfusion (MP) abnormalities in patients with diseases that are known or suspected to have myocardial microvascular involvement. The specific aims for each study (I - IV) are listed below.

I To determine if global MP during adenosine stress is reduced in young patients both at risk of developing, and fully developed hypertrophic cardiomyopathy (HCM) compared to healthy controls. The study also aimed to determine if MP correlates with diastolic dysfunction in the investigated patients.

II To determine if global MP during adenosine stress is reduced in patients with systemic sclerosis (SSc) compared to healthy controls.

III To determine if patients with suspected microvascular angina (MVA) have lower global MP during adenosine stress compared to healthy controls and coronary artery disease (CAD) patients, and to determine if there are sex differences of global MP within the groups.

IV To determine normal reference values for global MP at rest and adenosine stress by measuring the coronary sinus (CS) flow with MRI in healthy controls. The study also aimed to determine the accuracy of the MRI sequence used for CS flow measurements with a phantom experiment.

Chapter 3

Materials and methods

All four studies included in this thesis were approved by the regional ethics committee, Lund, Sweden. In all four studies, written informed consent was obtained from the persons participating in the studies. For Study I, written informed consent was also obtained from the parents if the patient was a minor.

Patients were recruited to all studies from the clinical throughput at Lund University Hospital, and healthy volunteers were recruited to all four studies. Study II-IV constituted both coronary sinus (CS) flow data from newly recruited healthy volunteers and CS flow data that had been previously published by coauthors to the current study[98]. An overview of the persons included in the four studies are shown in Figure 3.1

3.1 Study populations

Study I recruited patients with established hypertrophic cardiomyopathy (HCM) or risk of developing the disease. The following criteria were used to classify the participants into three study groups: (i), "HCM" if the interventricular septum and/or posterior wall thickness exceeded 13 mm (young adults, >18 years of age) or >3 SD on Z-score (pediatric patients) on echocardiography with confirmed myocardial hypertrophy and/or fibrosis on magnetic resonance imaging (MRI); (ii), "HCM risk" if the disease was present among first-degree relatives, but with normal morphology on MRI. In total, 10 HCM patients (2 women, age 22.3 ± 6.4 years), 14 HCM risk (7 women, 18.9 ± 3.8 years), and 12 healthy controls (3 women, 22.8 ± 4.5 years) were included in the study (Table 3.1).

Study II recruited patients diagnosed with SSc in compliance with the American College of Rheumatology/European League against Rheumatism 2013 classification [99]. 19 SSc patients (17 women, age 61 ± 10 years) and 22 healthy controls (10 women, 62 ± 11 years) were included in the study (Table 3.2).

Study III recruited both patients with suspected microvascular angina (MVA) and patients with established coronary artery disease (CAD). The following criteria classified par-

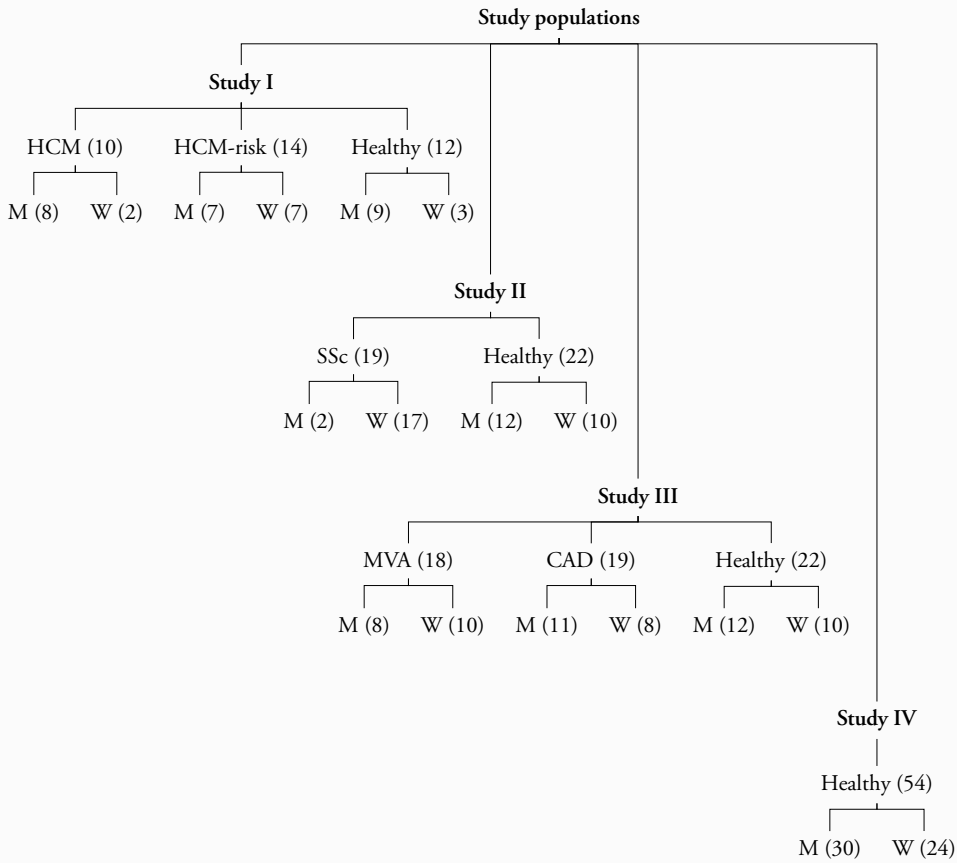

Figure 3.1: Overview of the patients included in the four studies of this thesis. All healthy volunteers included in study II were also included in study III. All healthy volunteers included in study I, II, and III were also included in study IV. The group sizes are written in parentheses. M = men, W = women, HCM = hypertrophic cardiomyopathy, Healthy = healthy controls, SSc = systemic sclerosis, MVA = suspected microvascular angina, CAD = coronary artery disease.

	Controls (n = 12)	HCM-risk (n = 14)	HCM (n = 10)
Age (years)	22.8 ± 4.5	18.9 ± 3.8	22.3 ± 6.4
Men	9 (75%)	7 (50%)	8 (80%)
BSA (m^2)	1.9 ± 0.1	1.8 ± 0.05	2.0 ± 0.1
Beta blockers	0	0	3
EDV/BSA (mL/m^2)	110 ± 5	89 ± 3*	91 ± 6*
ESV/BSA (mL/m^2)	49 ± 3	38 ± 2*	39 ± 6*
Ejection fraction (%)	55 ± 2	57 ± 1	59 ± 3
LVM/BSA (g/m^2)	56 ± 3	46 ± 2*	75 ± 12†
Left atrial size (mL)	82 ± 11[a]	64 ± 4	90 ± 6†[b]
Max IVS thickness (mm)	8.9 ± 0.5	8.5 ± 0.3	19.0 ± 2.4*†
Max PW thickness (mm)	7.2 ± 0.4	6.6 ± 0.2	9.6 ± 1.0*†

Table 3.1: Patient characteristics for the participants in the hypertrophic cardiomyopathy (HCM) study (Study I). BSA = body surface area, EDV = end diastolic volume, ESV = end systolic volume, IVS = interventricular septum, PW = posterior wall. * $P < 0.05$ compared to controls, † $P < 0.05$ compared to patients at HCM-risk, [a] n = 10, [b] n = 9 due to incomplete coverage of the left atrium. Data are presented as mean ± SEM.

	Controls (n = 22)	SSc-patients (n = 19)
Age (years)	62 ± 11	61 ± 10
Men	12 (55%)	2 (11%)
BMI (kg/m^2)	25 ± 3	26 ± 5
LVM/BSA (g/m^2)	58 ± 11	54 ± 12
EDV/BSA (g/m^2)	84 ± 12	76 ± 12*
ESV/BSA (g/m^2)	32 ± 8	27 ± 7
CI (L/min/m^2)	3.2 ± 0.4	3.6 ± 0.6
Skin involvement		
diffuse		7
limited		12
Disease duration (years)		10 ± 6
Antibody		
ANA		6
ACA		5
ARA		5
ATA		6
PAH		1
VC % expected		96 ± 12
DLCO % expected		80 ± 19
VC % predicted/DLCO % predicted		1.3 ± 0.3
Uric acid (µmol/L)		262 ± 59
Telangiectasias		14
Pitting scars		5
Nailfold CD (loops/mm)		5.0 ± 1.3
Skin score < 10		18
Skin score 10–20		1
Skin score > 20		1
Nifedipine		12
ERA		2
PDE5I		5

Table 3.2: Patient characteristics for the participants in the systemic sclerosis study (Study II). BSA = Body surface area, BMI = Body mass index, LVM = left ventricular mass, EDV = end diastolic volume, ESV = end systolic volume, CI = cardiac index, PAH = pulmonary arterial hypertension, VC = vital capacity, DLCO = diffusing capacity of the lung for carbon monoxide, ANA = anti nuclear antibodies other than ACA, ARA or ATA, ACA = anti centromeric antibodies, ARA = anti RNA polymerase III antibodies, ATA = anti topoisomerase I antibodies, CD = capillary density, ERA = endothelin receptor antagonist, PDE5I = phosphodiesterase type 5 inhibitor. * $P < 0.05$. Data are presented as mean ± SD.

ticipants into the different in the study groups: (i), "suspected MVA" patients with a history of angina pectoris and pathological ST-T reaction on a bicycle exercise stress test, but normal findings on myocardial perfusion single photon emission computed tomography (MPS), normal first-pass perfusion MRI, and no myocardial infarction on late gadolinium enhancement (LGE) MRI; (ii), "CAD patients" with verified coronary artery disease defined as a significant coronary artery stenosis on angiography, and/or stress-induced ischemia on MPS, or stress-induced ischemia on CMR. 18 patients with suspected MVA (65 ± 11 years), 19 CAD patients (69 ± 5 years), and 22 healthy volunteers (62 ± 11 years) were included in the study (Table 3.3).

Study IV, that aimed to determine determine normal reference values for MRI CS flow derived global myocardial perfusion (MP), included 54 healthy volunteers (age range 16-84 years, 24 women) (Table 3.4).

3.2 Magnetic resonance image acquisition and analysis

In all four studies, 1.5 Tesla MRI scanners with 32-channel coils were used. Due to scheduled MRI scanner replacement at the department, different scanners were used in the studies. In Study I, a Philips Achieva (Philips Healthcare, Best, the Netherlands) was used. In Study II-IV, the Philips Achieva or a Siemens Magnetom Aera (SiemensHealthcare GmbH, Erlangen, Germany) were used.

3.2.1 MRI image analysis

All MRI images were analyzed using the freely available image analysis software Segment (Medviso, Lund, Sweden) [100].

3.2.2 Left ventricular mass and function

In all four studies, 2-, 3-, and 4-chamber and short-axis cine images of the heart were acquired with an steady-state free precession MRI (SSFP) sequence during end-expiratory breath-hold. MRI image parameters are shown in Table 3.5.

The left ventricular (LV) endocardial and epicardial border of the LV were manually delineated in the short-axis cine images at both end-systole and end-diastole performed (Figure 3.2). Anatomical landmarks from the 2-, 3-, and 4-chamber images were used to improve the delineations' precision in the short-axis images. LV mass was calculated as the average end-systolic and end-diastolic myocardial volume and multiplied by 1.05 g/mL (myocardial density). The end-diastolic volume (EDV) and end-systolic volume (ESV) were measured as the enclosed volume by the endocardial delineation at its respective moment in the cardiac cycle. The stroke volume was calculated as EDV - ESV, and the cardiac output was calculated as stroke volume multiplied by heart rate.

	Controls (n = 22)	Suspected MVA (n = 18)	CAD patients (n = 19)
Age (years)	62 ± 11	65 ± 11	69 ± 5
Men	12 (55%)	8 (44%)	11 (58%)
LVM/BSA (g/m^2)	58 ± 11	57 ± 15	61 ± 13
EDV/BSA (g/m^2)	84 ± 12	76 ± 16	84 ± 19
ESV/BSA (g/m^2)	32 ± 8	24 ± 6*	35 ± 20
EF (%)	64 ± 10	68 ± 4*	61 ± 13
CI (L/min/m^2)	3.2 ± 0.4	3.5 ± 0.9	3.4 ± 0.8
Medications			
Oral nitrates	0	6	13
Acetyl salicylic acid	0	7	16
Clopidogrel	0	0	4
Ticagrelor	0	1	4
Beta blockers	0	9	11
Ca-channel antagonists	0	5	9
Statins	0	5	17
ACE-inhibitors	0	7	12
Diagnoses			
Hypertension	0	10	11
Hypercholesterolemia	0	5	11
Diabetes	0	3	5
Adenosine/bicycle exercise MPS	0/0	7/11	16/3
Philips/Siemens CMR	11/11	5/13	14/5

Table 3.3: Patient characteristics for the participants in the patients with suspected microvascular angina (MVA) study (Study III). CAD = coronary artery disease, BSA = body surface area, LVM = left ventricular mass, EDV = end diastolic volume, ESV = end systolic volume, CI = cardiac index. * $P < 0.05$ compared with healthy volunteers. Data are presented as mean ± SD.

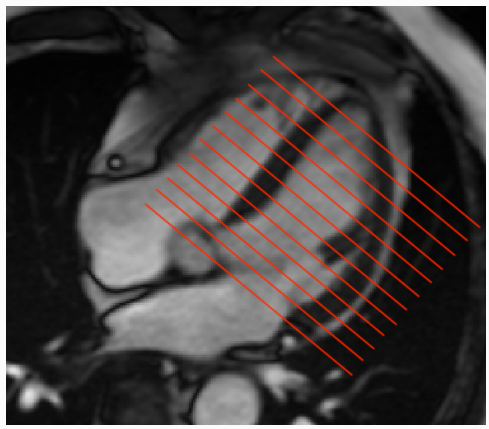

(a) 4-chamber image of the left ventricle.

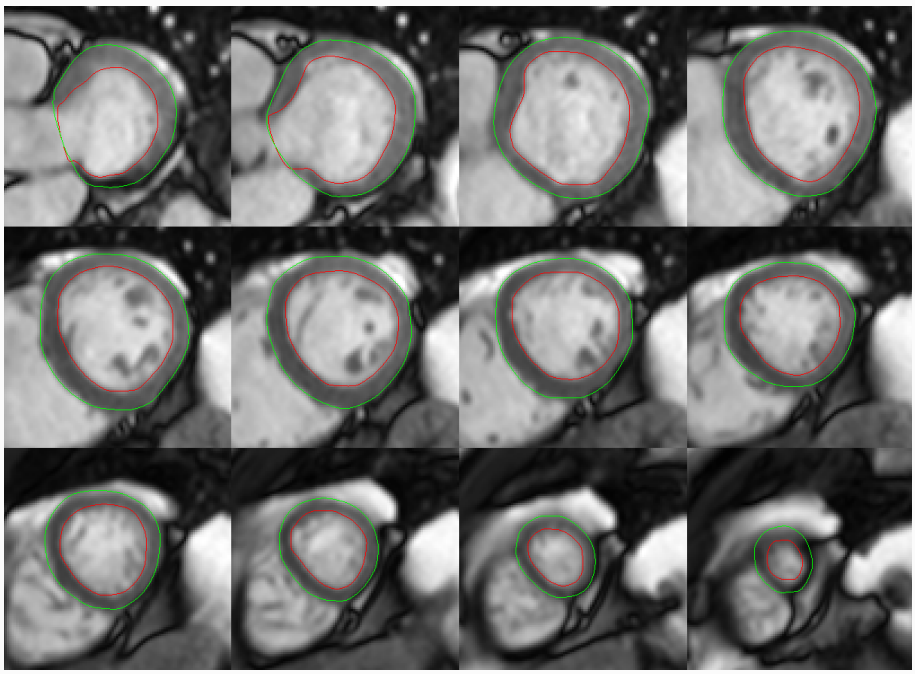

(b) Short-axis images of the left ventricle

Figure 3.2: (a) Typical 4-chamber image at end-diastole of the left ventricle (LV) with the positioning of the short-axis (SA) image planes marked with red lines (b) Corresponding SA images with endocardial (red) and epicardial (green) manual delineations.

	Women (n = 24)	Men (n = 30)
Age (years)	54 ± 17	48 ± 20
LVM (g)	85 ± 17	134 ± 26*
LVM/BSA (g/m^2)	50 ± 11	65 ± 11*
EDV (mL)	138 ± 23	196 ± 35*
EDV/BSA (mL/m^2)	81 ± 13	95 ± 17*
ESV (mL)	54 ± 15	78 ± 21*
ESV/BSA (mL/m^2)	32 ± 9	38 ± 10*
SV (mL)	84 ± 15	117 ± 22*
SV/BSA (mL/m^2)	50 ± 8	57 ± 10*
Cardiac output (L/min)	5.5 ± 1.1	7.1 ± 1.8*
Cardiac index (L/min/m^2)	3.3 ± 0.8	3.4 ± 0.8

Table 3.4: Left ventricular characteristics according to gender for the healthy volunteers participating in Study IV. LVM = left ventricular mass, BSA = Body surface area, EDV = end diastolic volume ESV = end systolic volume, SV = stroke volume. Data are presented as mean ± SD. * P < 0.05.

3.2.3 Coronary sinus flow derived global myocardial perfusion

The CS flow image plane was planned with guidance from a basal short-axis image of the LV. The image plane was placed as a cross-section to the coronary sinus and closely to the orifice in the right atrium to include the middle cardiac vein (Figure 3.3). CS flow was measured at rest and after 4-5 min of adenosine (Life Medical, Stockholm, Sweden) infusion (140 mg/kg/min) using a phase-encoded breath-hold turbo field echo velocity mapping sequence. This method to measure coronary sinus flow has previously been validated and used in a variety of studies [20, 98, 101] and is further validated in Study IV of this thesis. Typical MRI image parameters for cine and CS flow imaging are shown in Table 3.5.

The CS was manually delineated through all time frames, and quantitative flow measurements were extracted. Using these measurements, global MP (mL/min/g) was calculated as CS flow/LV mass. In study IV, CS flow derived global MP values at rest were also presented with adjustment to rate pressure product using the formula 10000 × global MP / systolic blood pressure × heart rate[102] to account for differences in external cardiac workload.

3.2.4 First-pass perfusion (regional myocardial perfusion)

Regional MP images was acquired in Study I and Study III using an SSFP first-pass perfusion sequence. A bolus of 0.05 mmol/kg gadolinium-based contrast agent (gadoteric acid,

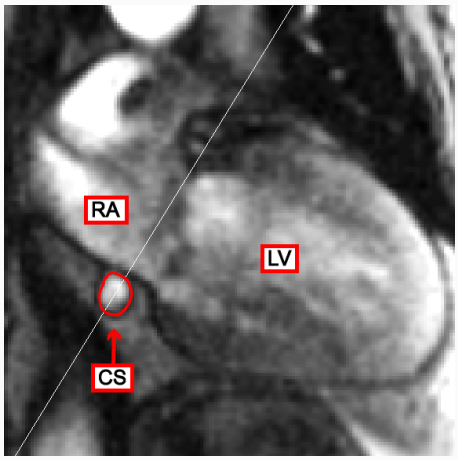

(a) Coronary sinus magnitude image.

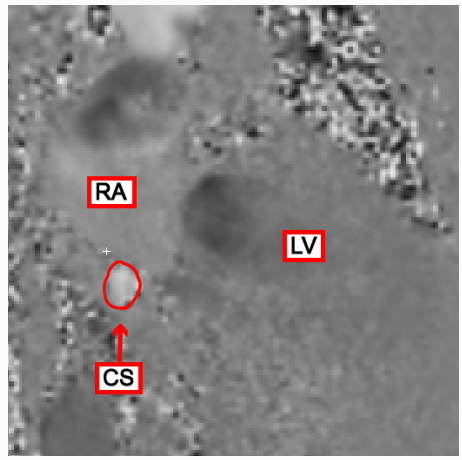

(b) Coronary sinus phase image.

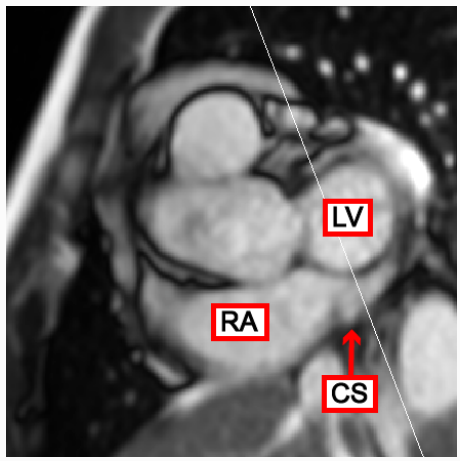

(c) Placement of the coronary sinus image plane.

Figure 3.3: (a) Magnitude image of the coronary sinus. (b) Flow velocity encoded image of the coronary sinus flow. (c) Short-axis image of the right atrium and coronary sinus ostium with a thin white line that marks the coronary sinus image plane. CS = coronary sinus, RA = right atrium, LV = left ventricle.

	Coronary sinus flow		Cine imaging	
	Philips	Siemens	Philips	Siemens
Repetition time (ms)	5	5	2.9	2.5
Echo time (ms)	2.6	2.8	1.5	1.1
Flip angle (degrees)	15	20	60	69
Inversion time (ms)	n/a	n/a	n/a	n/a
Segmentation factor	4	4	17	17
Acq. spatial res. (mm)	2.1×2.1×7.0	1.7×1.9×8.0	2.0×2.0×8.0	2.2×2.2×6.0-8.0
Reconstr. spatial res. (mm)	1.2×1.2×7.0	1.6×1.6×8.0	1.3×1.3×8.0	2.2×2.2×6.0-8.0
Acq. temporal res. (ms)	34	40	50	40
Reconstr. time phases	20	20	30	25
SENSE/GRAPPA factor	2	2	2	2
VENC (cm/s)	80-120	80-120	n/a	n/a
Slice gap (mm)	n/a	n/a	0	0-2

Table 3.5: MRI sequence parameters for coronary sinus flow measurements and cine imaging of the left ventricle. SENSE = sensitivity encoding, GRAPPA = generalized auto-calibrating partial parallel acquisition, VENC = velocity encoding.

Dotarem, Guerbet, Gothia Medical AB, Billdal, Sweden) was used. Images were sampled in three short-axis slices (base, mid-ventricular, and apical) during adenosine stress (140 mg/kg/min) and at rest, 10 minutes after the adenosine infusion was ended.

The first-pass perfusion images were visually analyzed in six basal, six mid-ventricular, and four apical segments. Each segment was graded regarding the deficit's transmural extent in each segment (< 50% or > 50%). The severity of the perfusion deficit was graded as mild/moderate or severe based on the observer's visually estimated hypo-enhancement degree.

3.2.5 Late gadolinium enhancement (fibrosis)

Myocardial fibrosis was measured in Study I, II and III using LGE. LGE imaging was performed with a 3D-inversion recovery (IR) gradient-echo (GRE) sequence (Philips) or 2D phase-sensitive inversion recovery (PSIR) GRE sequence (Siemens) acquired during end-expiratory breath-hold. Short-axis slices covering the entire left ventricle from base to apex and three long-axis projections were acquired 10–20 minutes after an intravenous administration of an additional 0.1 mmol/kg of contrast agent after the resting perfusion (Figure 3.4). MRI image parameters are shown in Table 3.6.

In Study I and II, fibrosis was quantified using a semi-automatic method of the LGE images using threshold by SD from remote with manual corrections[103]. In Study III, a

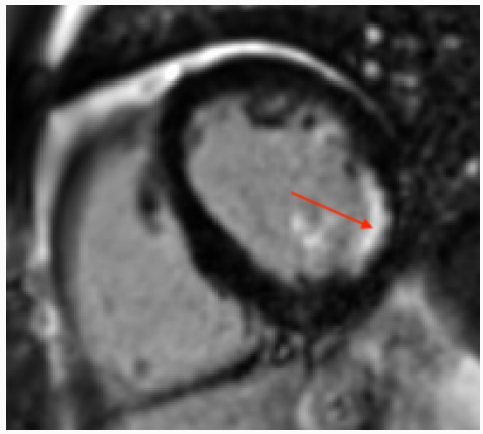

Figure 3.4: Typical short-axis basal late gadolinium enhancement MRI image with fibrosis (marked with an arrow) as a result of myocardial infarction in the LCx territory in a patient with coronary artery obstructions in LAD, RCA and LCx on angiography

later developed method using threshold by expectation maximization to semi-automatically include fibrosis areas was used[104].

3.3 Phantom-experiment design

In Study IV, a phantom was assembled to validate the CS flow sequence against a computer controlled mechanical fluid pump (Figure 3.5). The phantom consisted of a plastic bowl penetrated by four thin-walled (0.1-0.25 mm) plastic tubes with increasing inner diameters (4.7, 5.8, 6.5, and 7.7 mm), serially connected to a custom made pulsating pump and placed in the middle of the MRI scanner. The pump consisted of a linear actuator attached to a compressor-chamber through which it exerted cyclic force to the fluid compartment. Unidirectional flow was achieved by one-way valves on each side of the compressor-chamber. The system was filled with tap water doped with manganese chloride (0.27 mM/liter) to resemble the T1-value of blood. The stroke volume of the pump was gradually increased to achieve a set of different flow-velocities in the four tubes. The pump-rate was dialed to 80 cycles/minute, which was considered to mimic a physiological heart-rate. The phantom was scanned in the Siemens Magnetom Aera scanner with the same velocity-mapping sequence used for CS flow measurements in the clinical studies.

(a) Phantom with thin-walled vessels

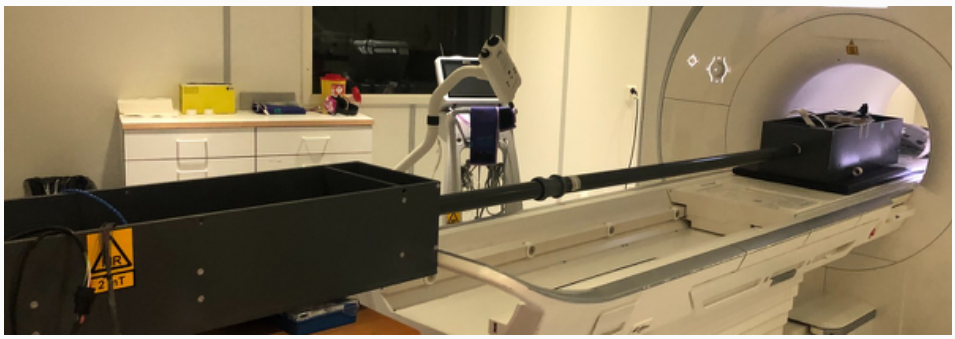

(b) Mechanical pump setup

Figure 3.5: (a) Photo of the phantom consisting of a plastic bowl penetrated by four thin-walled (0.1-0.25 mm) plastic tubes with increasing inner diameters (4.7, 5.8, 6.5, and 7.7 mm). (b) Photo of the pump with the computer controlled linear actuator on the left side avoiding the strong magnetic field. The compressor-chamber and fluid compartment are inside the magnetic core.

	Regional perfusion		LGE	
	Philips	Siemens	Philips	Siemens
Repetition time (ms)	2.7	2.3	4.2	8.3
Echo time (ms)	1.4	1.0	1.3	3.2
Flip angle (degrees)	50	50	15	25
Inversion time (ms)	220-280	110	220-280	300
Segmentation factor	n/a	69	49	20
Acq. spatial res. (mm)	2.0×2.0×10.0	2.4×2.8×8.0	1.5×1.5×8.0	1.3×1.8×8.0
Reconstr. spatial res. (mm)	1.4×1.4×10.0	2.4×2.4×8.0	1.5×1.5×8.0	1.3×1.3×8.0
Acq. temporal res. (ms)	n/a	159	n/a	n/a
SENSE/GRAPPA factor	3	2	0	2
Number of slices/heartbeat	5	3	n/a	n/a
Slice gap (mm)	Individual	Individual	0	2

Table 3.6: MRI sequence parameters for first-pass perfusion and late gadolinium enhancement (LGE). SENSE = sensitivity encoding, GRAPPA = generalized auto-calibrating partial parallel acquisition.

3.4 Bicycle exercise test

In Study III, a bicycle exercise stress test was performed using a bicycle ergometer. Starting load and increment were based on age, sex, and self-estimated fitness, typically starting at 30-60W with 10-20W/min load increments until exhaustion[105]. Two expert readers analyzed the test results, and ST-T response was considered pathological if there was more than 1 mm of stress-induced ST depression with a horizontal or downward sloping ST-segment, or ST changes after 4 minutes of recovery were seen in the lateral chest leads (V4-V6).

3.5 Statistical analysis

In Study I-IV, statistical analysis was performed using GraphPad Prism (GraphPad Software Inc, San Diego, CA, USA). In Study II-IV, statistical analysis was also performed using IBM SPSS (IBM Corp, Armonk, NY, USA) in conjunction with GraphPad Prism (GraphPad Software Inc, San Diego, CA, USA).

In Study I, data were reported as mean ± standard error of the mean. In Study II-IV, the data was reported as mean ± standard deviation. In Study I-II, the group means were compared using the Mann-Whitney non-parametric test. In Study III, the group means were compared using the non-parametric Kruskal-Wallis test with Dunn's test post hoc, and in Study IV, the parametric independent-samples t-test was used. Correlations were analyzed in Study I and Study IV with either Spearman's rank-order test or Pearson's bivariate correlation test. The Bland–Altman method was used to analyze the agreement

between methods. In all four studies, differences with $P < 0.05$ was regarded as statistically significant.

Chapter 4

Results and comments

The major findings of each study are presented and discussed in this chapter. More detailed information is found in each manuscript in part II at the end of the thesis summary.

4.1 Study I - Cardiac microvascular disease in HCM

Hypertrophic cardiomyopathy (HCM) is the most frequent cause of sudden death in children[106] and athletes[107]. A low myocardial perfusion (MP) has previously been reported in studies investigating adult patients[54–56, 108], and it has been shown that a low MP is a strong predictor of increased clinical severity and death in adult patients with HCM [56]. Understanding the mechanisms that cause the increased risk of major adverse events in young HCM-patients is crucial for the long term goal of preventing and treating the disease. When Study I was planned, there was no data available on global MP in children and adolescents with HCM (HCM-patients) or risk of developing the disease (HCM-risk). Therefore, we aimed to investigate the global MP in a group of pediatric HCM-patients.

Table 4.1 shows the heart rate, blood pressure, and global MP at rest and adenosine stress and Figure 4.2 shows the individual global MP values at rest and stress in scatter plots. At rest, there was no significant difference in MP between the healthy controls, HCM-risk, and HCM-patients. During adenosine stress, MP was significantly lower in HCM-patients than HCM-risk and healthy controls. There was no significant difference in global MP between patients with HCM-risk and healthy controls during adenosine stress.

Our finding of lower global MP during adenosine stress in HCM-patients as a sign of coronary microvascular dysfunction (CMD) is coherent with a previous study by Petersen et al.[109] using quantitative first-pass perfusion magnetic resonance imaging (MRI) to investigate adult patients. More specifically, Petersen et al.[109], showed that global MP at rest is similar in adult HCM-patients (0.71 ± 0.27 mL/min/g) and controls (0.85 ± 0.30

		Controls	HCM-risk	HCM
Rest	Heart rate (BPM)	59 ± 4	67 ± 2*	74 ± 4*
	Systolic BP (mmHg)	117 ± 3	112 ± 3	116 ± 3
	Diastolic BP (mmHg)	66 ± 2	64 ± 2	64 ± 3
	Global MP (mL/min/g)	0.8 ± 0.1	1.0 ± 0.1	0.9 ± 0.1
Stress	Heart rate (BPM)	95 ± 4	98 ± 4	101 ± 5
	Systolic BP (mmHg)	114 ± 3	109 ± 3	114 ± 4
	Diastolic BP (mmHg)	68 ± 2	62 ± 2	69 ± 4
	Global MP (mL/min/g)	3.9 ± 0.3	5.0 ± 0.5	2.5 ± 0.4†*

Table 4.1: Hemodynamic response at rest and during adenosine stress in healthy controls and HCM-patients. BPM = beats/minute, MP = Myocardial perfusion. Data are presented as mean ± SEM. * = $P < 0.05$ compared to heathy controls, † = $P < 0.05$ compared to patients at risk of developing HCM

mL/min/g), but that global MP at stress is lower in HCM-patients (1.84 ± 0.89 mL/min/g) than in healthy controls (3.42 ± 1.76 mL/min/g).

Though the finding of lower global MP during adenosine stress compared to healthy controls in the children and adolescents participating in our study is similar to that of adults reported by Petersen et al.[109], our global MP values are consistently lower, both for controls and HCM-patients. This could be due to: (a), age differences in global MP seen as lower values in the population in our study, or; (b), underestimation of global MP by quantitative first-pass perfusion, or (c) overestimation of coronary sinus (CS) flow derived global MP, or a combination of a, b and, c. Study IV of this thesis investigate age differences in global MP in healthy volunteers and reports no decline in global MP with age. However, additional studies are needed to determine potential age differences in global MP in HCM-patients.

As discussed in the introduction chapter, the myocardium is normally perfused mainly during the diastolic phase of the cardiac cycle. To investigate during what portion of the cardiac cycle in which the myocardial blood flow is constricted, averaged coronary sinus flow curves from the three study groups were plotted (Figure 4.1). These flow curves reveal that altered flow patterns accompany the lower global MP observed in the HCM-patients. More specifically, the normal biphasic flow during adenosine stress in healthy persons is replaced by a more even CS flow in HCM-patients.

We hypothesized that such a flattened flow curve could be due to left ventricular (LV) diastolic dysfunction where a prolonged diastole affects the perfusion during the diastolic phase of the cardiac cycle. However, we were not able to test this hypothesis since only one HCM-patient was found to have an $E/e' > 15$ on echocardiography, which was considered the cutoff for the potential of a diastolic dysfunction to generate an increased left ven-

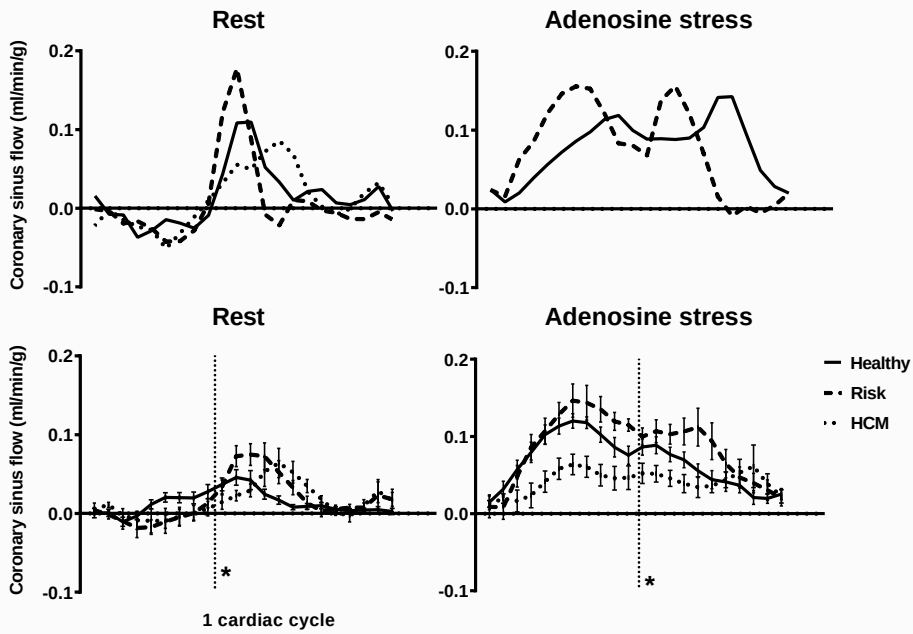

Figure 4.1: Top panels: Typical coronary sinus (CS) flow curves at rest (top left panel) and adenosine stress (top right panel) for a healthy control (solid line), a subject at HCM-risk (broken line) and an HCM-patient (dashed line). Bottom panels: The average CS flow ± SEM for each group at rest (bottom left panel) and adenosine stress (right panel). The CS flow during adenosine stress is lower throughout the cardiac cycle in HCM-patients compared to healthy controls and patients with HCM-risk. * = Average end systole.

tricular filling pressure[110, 111]. As discussed in the introduction chapter, the common MYBPC3-mutation may contribute to the hyperdynamic systolic function commonly seen in HCM[112], which hypothetically could limit the myocardial blood flow during systole. However, this question needs to be addressed in future studies since our study only included 3 HCM-patients and 4 HCM-risk patients with MYBPC3-mutation, which is an insufficient population size for genetic subgroup stratification of the data.

Seven HCM patients had fibrosis on LGE (5 ± 1% fibrosis of the LV mass). There was no correlation between degree of fibrosis and global myocardial perfusion during stress. No controls or patients at HCM risk had fibrosis.

Six patients with a total of 30/126 segments (24%) were found to have a perfusion defect during adenosine stress. Out of the 30 segments with perfusion defects, subendocardial perfusion defects where seen in 12 segments, in which 11 were mild and one was

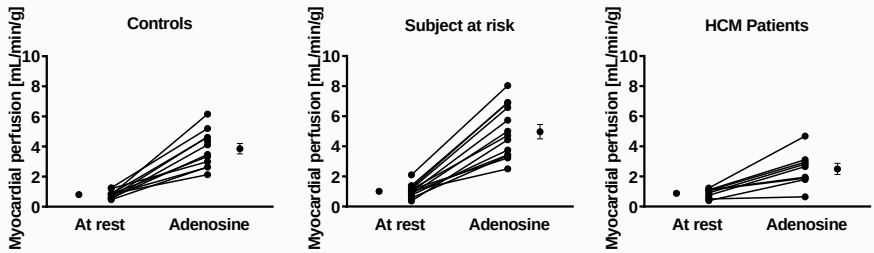

Figure 4.2: Global myocardial perfusion (MP) at rest and during adenosine stress for each individual in all three groups. Global MP was significantly lower during adenosine in HCM patients compared to controls and subjects at HCM risk. Error bars = mean ± SEM.

severe. The remaining 18 segments had transmural perfusion defects, in which six were mild and 12 were severe. As mentioned in the introduction chapter of this thesis, Ismail et al. have reported that about 1/3 of adult HCM-patients show severe microvascular dysfunction when investigated with quantitative first-pass perfusion imaging and that the areas with severe microvascular dysfunction not only fails to increase during adenosine stress, but decreased compared to the resting value[57]. Future studies combining quantitative first-pass perfusion imaging and global MP from CS flow measurements in young HCM would therefore be of interest.

Coronary angiography were not performed in our study and therefor obstructive epicardial coronary artery disease (CAD) may not be ruled out as a cause a low global MP in the investigated patients. However, epicardial CAD is rarely seen in young individuals and coronary arteries may even have an increased diameter in HCM-patients[113]. The risk of unknown epicardial CAD impacting the results is therefore considered low. Nevertheless, coronary angiography may be considered in future studies investigating CMD in HCM patients to rule out epicardial obstructive CAD.

Left ventricular outflow tract gradients and E/e′ were only measured at rest. Hypothetical left ventricular outflow tract gradients and high E/e′ at stress can therefore not be ruled out as factors affecting global MP at stress. Almost all known young patients with HCM willing to participate in the uptake area of the clinic were included in the study. Yet, the study population is small, and because of that, the results of Study I in this thesis need to be confirmed in larger studies.

To summarize, Study I showed that pediatric patients with manifest HCM, but not those only with a hereditary risk of the disease, have lower global MP during adenosine stress than healthy controls. This finding is interpreted as CMD, which suggests that cardiac microvascular disease is prevalent in young HCM-patients.

4.2 Study II - Cardiac microvascular disease in SSc

SSc is a severe and biologically complex disease with multi-organ involvement[58]. From a cardiovascular perspective, patients with systemic sclerosis (SSc) have an increased frequency of cardiovascular mortality[62] even though there is little to no increase in epicardial CAD[63, 114].

In a study using myocardial perfusion single photon emission computed tomography (MPS), eight of ten SSc-patients with exercise-induced perfusion abnormalities were examined with coronary angiography, but none was found to have epicardial CAD[115]. This suggests that patients SSc may suffer from cardiac microvascular disease affecting microvascular coronary circulation. Therefore we aimed to determine if patients with SSc have lower global MP at rest and during adenosine stress compared to healthy controls, as a measure of CMD.

Table 4.2 shows the heart rate, blood pressure, and global MP at rest and adenosine stress in patients with SSc and healthy controls. Figure 4.3 shows the individual global MP values at rest and stress in a scatter plot. At rest, there was no significant difference in global MP between patients and controls. During adenosine stress, however, SSc-patients showed a significantly lower global MP compared to healthy controls. In our study, the coronary flow reserve (CFR) was significantly lower i the SSc-patients compared to the healthy volunteers (3.5 ± 1.9 vs. 4.3 ± 1.1, P = 0.09). Our observation of lower global MP in patients with SSc are coherent with previous studies using coronary angiography and echocardiography[65, 116].

Recently, a first-pass perfusion MRI study by Gigante et al. using a rest/stress protocol in which the patients submerge their hands in zero to four degrees Celsius cold water for three minutes reported no difference in global MP between SSc-patients and healthy controls[117]. However, in the study by Gigante et al.[117], there was only a moderate increase in global MP at stress (23% in SSc-patients and 40% in healthy volunteers) compared to the large increase reported in our study using an adenosine rest/stress protocol. This suggests that an adenosine protocol induces a stronger hemodynamic response than a cold water protocol, which could contribute to the different results seen in Gigantes study[117] compared to ours.

There was no significant difference in global MP between diffuse cutaneous and limited cutaneous SSc at rest (0.9 ± 0.1 vs. 1.2 ± 0.2 mL/min/g), or during adenosine stress (3.0 ± 0.5 vs. 3.1 ± 0.2 mL/min/g).

Two SSc-patients had a substantially higher skin scores than the rest of the SSc-patients, and these two patients also were found to have the lowest global MP at stress (Patient_1 skin score = 14, stress global MP = 1.8 mL/min/g, and Patient_2 skin score = 49, stress global MP = 2.1 mL/min/g). This suggests that patients with more severe disease may suffer from worse CMD, but also that patients with mild disease may have a disturbed MP irrespective of the degree of fibrotic skin involvement. However, larger studies, including more patients with a higher skin score, are needed to test this hypothesis.

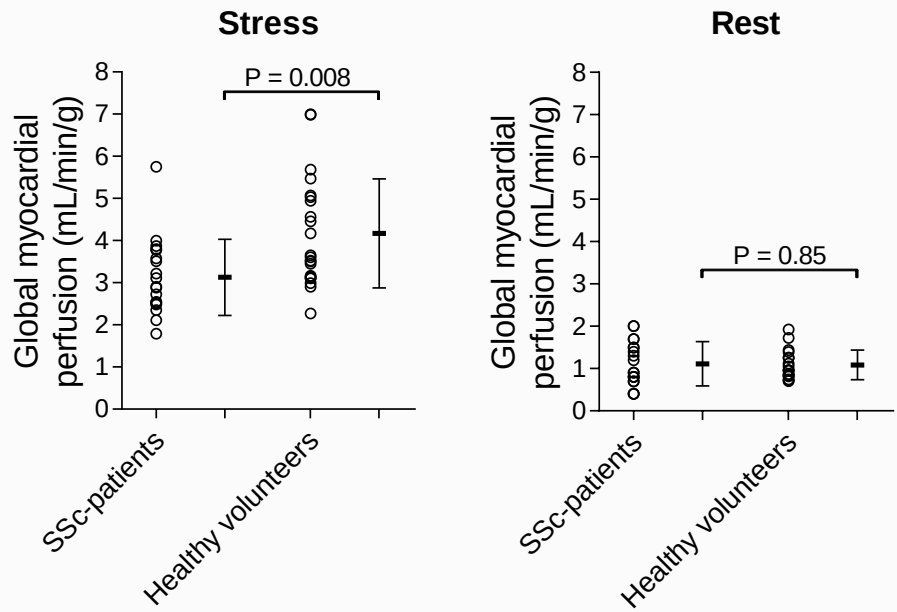

Figure 4.3: Global myocardial perfusion at rest and during adenosine stress for patients with SSc and healthy controls. There was a significant difference in myocardial perfusion during adenosine stress, but not at rest, between the healthy controls and the SSc-patients. Error bars = mean ± SD.

		Controls	SSc-patients
Rest	Heart rate (BPM)	65 ± 10	73 ± 11*
	Systolic BP (mmHg)	124 ± 13	127 ± 20
	Diastolic BP (mmHg)	73 ± 9	71 ± 13
	Global MP (mL/min/g)	1.1 ± 0.3†	1.1 ± 0.5
Stress	Heart rate (BPM)	85 ± 15	93 ± 13
	Systolic BP (mmHg)	124 ± 17	124 ± 19
	Diastolic BP (mmHg)	70 ± 11	65 ± 10
	Global MP (mL/min/g)	4.2 ± 1.3	3.1 ± 0.9*
	CFR	4.3 ± 1.1†	3.5 ± 1.9

Table 4.2: Hemodynamic response at rest and during adenosine stress in healthy controls and SSc-patients. BPM = beats/minute, MP = Myocardial perfusion. CFR = Coronary flow reserve. Data are presented as mean ± SD. * = $P < 0.05$ compared to heathy controls, † N = 18. Variables are presented as mean ± SD.

The nailfold capillary density was 5.0 ± 1.3 loops/mm, and there was no correlation between nailfold capillary density and MP at stress. This suggests that peripheral capillary involvement may not reflect the severity of CMD in SSc-patients.

late gadolinium enhancement (LGE) images were not obtained in three SSc-patients because of inability to withstand further scanning due to discomfort.

Three out of the 19 SSc-patients had septal fibrosis in the right ventricular insertion points, but none of these patients had signs of previous myocardial infarction (Figure: 4.4). Global MP at stress in the patients with fibrosis was at level with the other patients within the SSc group. Therefore it is likely that the fibrosis is a result of mechanical stress from a pre-clinical hypertensive pulmonary circulation, rather than an effect of local microvascular dysfunction.

First-pass perfusion imaging was not included in the study protocol of this study. However, the combination of first-pass perfusion and CS flow global MP would be of great interest to rule out regional hypoperfusion. Recent studies suggest that environmental factors such as silica dust, drugs, or infectious agents, may be risk factors for developing SSc[118, 119]. However, our study did not collect data about environmental factors, but future studies correlating such factors with CMD would be of interest. The number of included patients in the study was limited, mainly due to the rarity of patients with the disease. Because of this, the results of Study II need to be confirmed in larger studies.

To summarize, Study II showed that the global MP is lower in patients with SSc compared to controls. Finding non-invasive measures able to diagnose cardiac microvascular disease in SSc would be of high clinical and scientific value. CS flow derived global MP is a

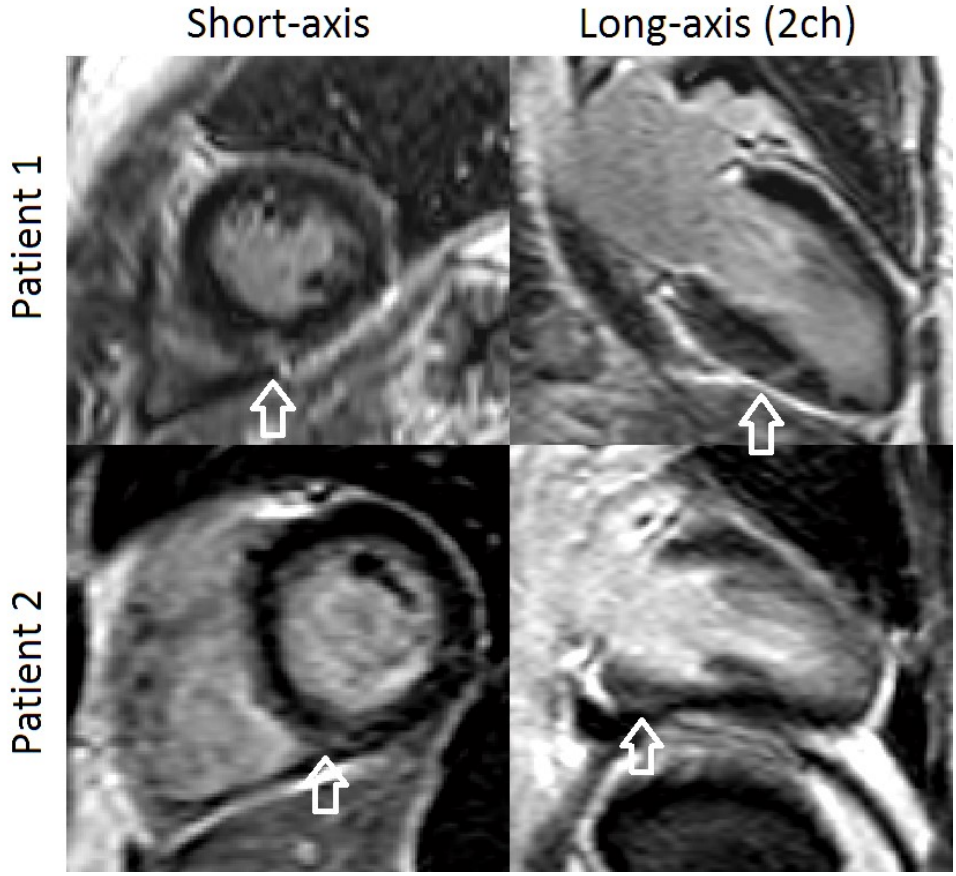

Figure 4.4: Late gadolinium enhancement (LGE) images showing fibrosis in the right ventricular insertion points in two patients with systemic sclerosis (SSc). The white arrows points to tissue with enhanced signal due to fibrosis.

candidate for this task, but further studies are needed to investigate the method's prognostic performance.

4.3 Study III - Cardiac microvascular disease in MVA

Coronary angiography or non-invasive MP imaging is usually performed to rule out stress-induced regional myocardial ischemia due to stenosis in the epicardial coronary arteries[69]. However, stress-induced chest-pain with regional MP defects on quantitative first-pass perfusion cardiac MRI may appear in the absence of significant coronary arterial stenosis[120]. This phenomenon has lately been called microvascular angina (MVA)[68] or ischemia and no obstructive coronary artery disease (INOCA)[71] and may be due to CMD.

In Study III, we sought to determine if patients with suspected MVA have lower global MP during adenosine stress compared to healthy controls and a group of CAD patients. Prevalence of MVA has been reported to be higher in women[69]. We therefore aimed to explore sex differences in global MP in the patients with suspected MVA.

Table 4.3 shows the heart rate, blood pressure, and global MP at rest and adenosine stress, and scatter plots of the same data are shown in figure 4.5. Due to insufficient image quality, global MP could not be measured in four of the healthy volunteers at rest. There were no significant differences in global MP between healthy controls, patients with suspected MVA, and CAD-patients at rest. During adenosine stress, patients with suspected MVA and CAD-patients showed a significantly lower global MP compared to healthy controls.

In our study, the mean CFR was significantly higher in patients with suspected MVA than the healthy controls and significantly lower in the CAD-patients than the healthy controls. This is likely due to the high variability in global MP at rest in the group of patients with suspected MVA, also resulting in high variability of the calculated CFR. Such a large variability in global MP at rest resulted in difficulties in establishing the lower limit of normal rest for positron emission tomography (PET) [121], and a wide range of regional CFR has been revealed in healthy individuals using MPS[122].

CFR is commonly used when investigating CMD, and in a large study of women with chest pain but no obstructive CAD, 26% of 963 symptomatic women were found to have a CFR below two, which was used as a cutoff value to indicated CMD when assessed by transthoracic Doppler echo[123]. A cut-off value of CFR < 2 has been shown to predict the long-term risk of major adverse clinical event (MACE) in both men and women[124, 125]. However, the risk of MACE is higher in men than women when using a cut-off value of CFR < 2 [16, 122] and a value of CFR < 2.32 to predict MACE in women has been suggested[126].

Furthermore, a reduction in coronary flow velocity reserve measured by Doppler echocardiography in the left anterior descending artery (LAD) has been shown to increase the hazard ratio with 7% per 0.1 unit decrease in coronary flow velocity reserve. This increase is mainly driven by an increased risk of myocardial infarction and heart failure[127].

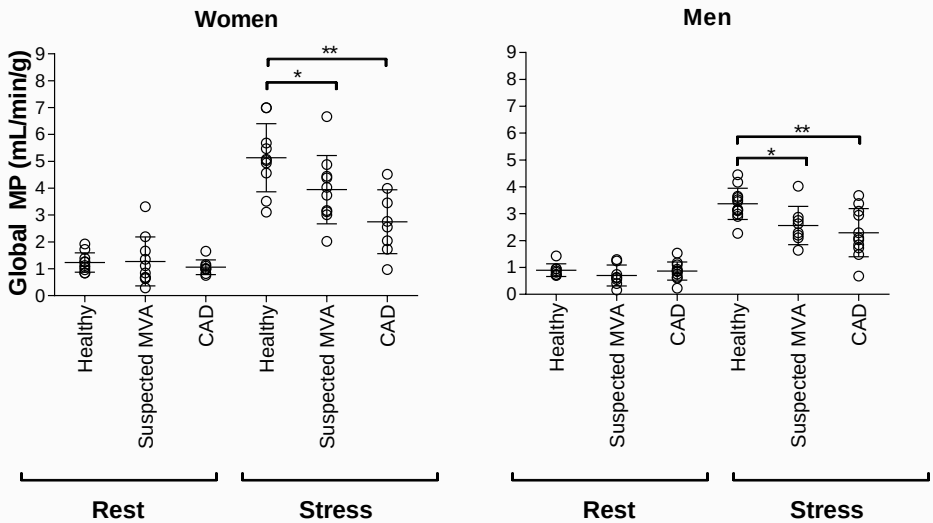

Figure 4.5: Global myocardial perfusion (MP) at rest and during adenosine stress in patients with suspected microvascular angina (MVA), patients with coronary artery disease (CAD) and healthy controls. Patients with suspected MVA showed lower global MP than healthy volunteers, but there was no difference between patients with suspected MVA and CAD patients. Error bars = mean ± SD. *P < 0.05, **P < 0.01.

	Controls	Suspected MVA	CAD-patients
Rest			
Heart rate (BPM)	65 ± 10	67 ± 11	68 ± 10
Systolic BP (mmHg)	124 ± 13	132 ± 22	136 ± 36
Diastolic BP (mmHg)	73 ± 9	77 ± 11	81 ± 12
Global MP (mL/min/g)	1.1 ± 0.3	1.0 ± 0.8	0.9 ± 0.3
Adenosine stress			
Heart rate (BPM)	85 ± 15	92 ± 14	86 ± 16
Systolic BP (mmHg)	124 ± 17	129 ± 17	132 ± 19
Diastolic BP (mmHg)	70 ± 11	73 ± 12	74 ± 14
Global MP (mL/min/g)	4.2 ± 1.3	3.3 ± 1.3*	2.5 ± 1.0*
Coronary flow reserve	4.3 ± 1.1	4.6 ± 3.0†	2.9 ± 1.7*

Table 4.3: Hemodynamic parameters at rest and during adenosine stress in healthy controls, patients with suspected microvascular angina (MVA) and patients with coronary artery disease (CAD). BPM = beats/minute, BP = blood pressure, MP = myocardial perfusion. Data are presented as mean ± SD. * = $P < 0.05$ compared to healthy controls, † $P < 0.05$ compared to CAD-patients.

In our study, both male patients with suspected MVA and male healthy controls had significantly lower global MP than women within the study groups. Potential sex differences in global MP are known and discussed in more detail in the next section about Study IV. In the present study, women with suspected MVA had lower global MP compared to healthy women, which is in line with previous studies[77, 128, 129].

Currently, invasive coronary angiography is not recommended when MPS is normal unless the patient has severe symptoms despite medication[71]. The presence of coronary artery stenosis in the patients with suspected MVA cannot be ruled out since they were included in the study based on a negative MPS and therefore invasive coronary angiography was not performed in any of the cases. However, the risk of unknown significant CAD is low given that the patients with suspected MVA included in the study had no regional hypoperfusion or signs of myocardial infarction on MRI. A final limitation of Study III that is worth noting is that the study population is relatively small and that the study thereby has limited power.

In conclusion, the findings in Study III show that patients presenting with suspected MVA have lower global MP than healthy volunteers and there is evidence of sex differences in global MP in patients presenting with suspected MVA that warrants further investigations.

4.4 Study IV - Normal CS flow derived global MP

CS flow measurement with MRI is well established, phantom-validated, and validated in-vivo both invasively and non-invasively[17, 20, 22, 130]. Although the technique has been available for almost three decades, there has been a lack of data on healthy volunteers. This may partly be due to historical dominance of cardiac PET for research on cardiac perfusion abnormalities in patients with suspected cardiac microvascular disease. However, with the recent technological advances that have increased the clinical utility of MRI for investigating cardiac microvascular dysfunction, the need for normal reference values in healthy subjects has increased to enable differentiation between health and disease in subjects with suspected but not yet diagnosed microvascular dysfunction.

In our study, there were no age-variations of heart rate at rest, but there was a lower heart rate in old compared to younger individuals during adenosine stress. A weaker heart rate response to adenosine in old persons has previously been shown in large studies and may be attributed to a attenuated baroreceptor reflex [124, 131]. The lack of age-variation of global MP during stress in our study is similar to a previous study by Czernin et al.[132] who found no correlation between global MP at dipyridamole stress in healthy volunteers using PET. However, the lack of age-variation of global MP during stress differs from other PET studies using dipyridamole stress that have shown that global MP at rest increases with age, and that global MP at stress declines with age[121, 133]. In the study by Uren et. al it is suggested that lower increase in global MP at stress in older persons is due to a less pronounced increase in heart rate[133]. In our study, however, we did not observe a decline in global MP despite that the heart rate decreased with age during adenosine stress for both genders.

Figure 4.7 shows the age variation of global MP for both genders, and Table 4.4 shows the mean values. At rest, men had a lower unadjusted and rate pressure product adjusted global MP compared to women. Men also had a lower global MP compared to women at adenosine stress. Such a sex-difference with higher global MP in women compared to men have recently been reported in a study by Nickander et al. using the quantitative first pass perfusion MRI technique [134].

Global MP did not vary with age for any of the genders. Since there was no correlation between age and global MP, subgroup categorization of different age ranges was not performed. Previous PET studies have not found a significant difference in global MP between the genders using dipyridamole[121, 135]. In our study, we used adenosine that has a higher vasodilator potency than dipyridamole[136]. In a study investigating coronary microvascular dysfunction with O-15-PET using an adenosine rest/stress protocol, 61 healthy male volunteers were included with reported values of global MP similar to our study (rest 0.87 ± 0.14 mL/min/g, stress 3.63 ± 1.2 mL/min/g)[137]. A higher increase in women than men in global MP during cold pressor tests has also been observed using MRI coronary sinus flow measurements in a study investigating young, healthy volunteers[5].

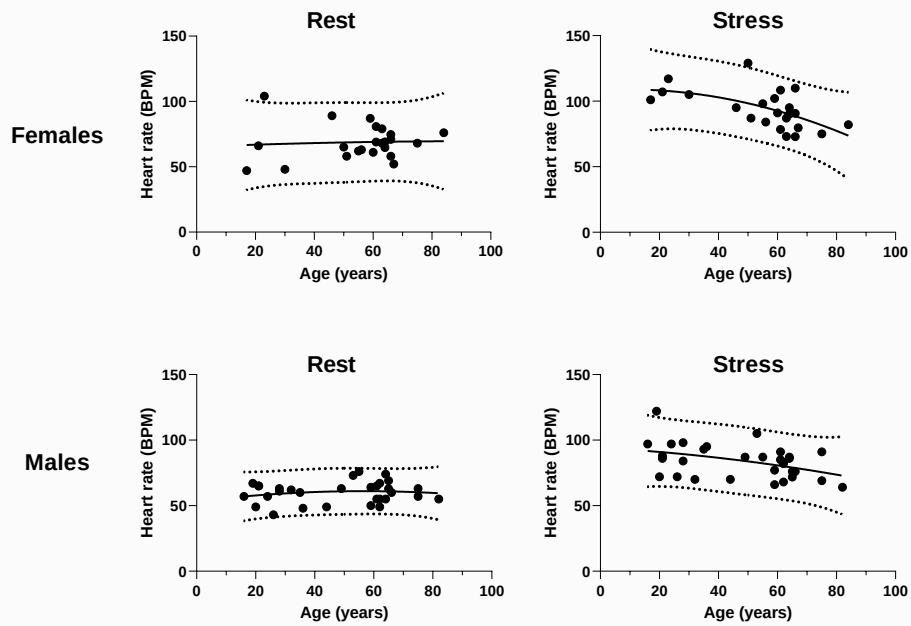

Figure 4.6: Heart rate at rest and adenosine stress vs. age according to gender. Solid line = quadratic regression line, dashed lines = 95% confidence interval. BPM = beats/min.

		Women	Men
Rest	Heart rate (BPM)	68 ± 13	60 ± 8*
	Systolic BP (mmHg)	123 ± 18	120 ± 12
	Diastolic BP (mmHg)	72 ± 11	72 ± 10
	Rate pressure product	8420 ± 2148	7218 ± 1201*
	Global MP (mL/min/g)	1.2 ± 0.4†	0.8 ± 0.3†*
	Corrected MP (mL/min/g)	1.4 ± 0.4†	1.1 ± 0.3†*
Stress	Heart rate (BPM)	94 ± 14	83 ± 13*
	Systolic BP (mmHg)	121 ± 17	122 ± 13
	Diastolic BP (mmHg)	70 ± 11	70 ± 10
	Global MP (mL/min/g)	4.9 ± 1.2	3.6 ± 0.9*
	Coronary flow reserve	4.4 ± 1.4†	5.4 ± 2.6†

Table 4.4: Hemodynamic response at rest and during adenosine stress in healthy men and women. BPM = beats/minute, MP = Myocardial perfusion. Data are presented as mean ± SD. * P < 0.05. † N = 23.

To verify the consistency of the manual image analysis between readers for global MP derived from coronary sinus flow measurements and LV segmentation, interobserver agreement was assessed in 10 cases at both rest and stress. The difference in global MP between the two observers was 0.1 ± 0.4 mL/min/g.

The mean error for MRI flow measurement vs. timer and beaker were 6 ± 3%, 2 ± 5%, –1 ± 4%, and –4 ± 5% for the Ø4.7 mm, Ø5.8 mm, Ø6.5 mm, and Ø7.7 mm pipe, respectively (Figure 4.8). The linear regression equations for MRI flow measurement vs. timer and beaker were Y = 1.12X - 5.08, Y = 1.08X - 5.36, Y = 1.03X - 4.33, and Y = 0.98 - 1.61 for the Ø4.7 mm, Ø5.8 mm, Ø6.5 mm, and Ø7.7 mm pipe respectively.

Study IV of this thesis reports age and gender-specific characteristics of CS flow derived global MP for healthy persons. The study also validated the CS flow method with a phantom-experiment that proved high accuracy and precision of the flow measurements.

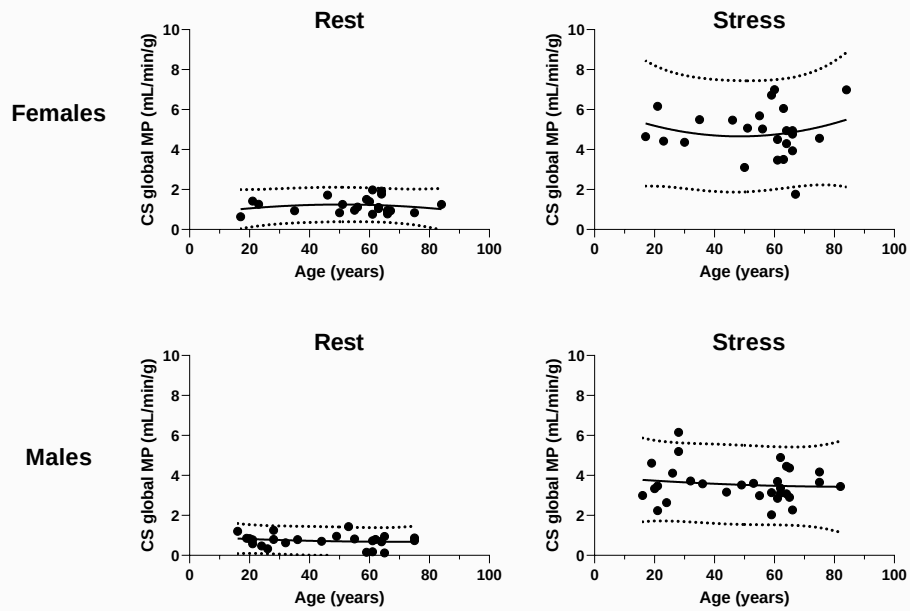

Figure 4.7: Coronary sinus (CS) global myocardial perfusion (MP) vs. age at rest and adenosine stress according to gender. There was no significant correlation between age and global MP, neither at rest nor during adenosine stress. Therefore, no further stratification of global MP based on age was performed. Solid line = quadratic regression line, dashed lines = 95% confidence interval.

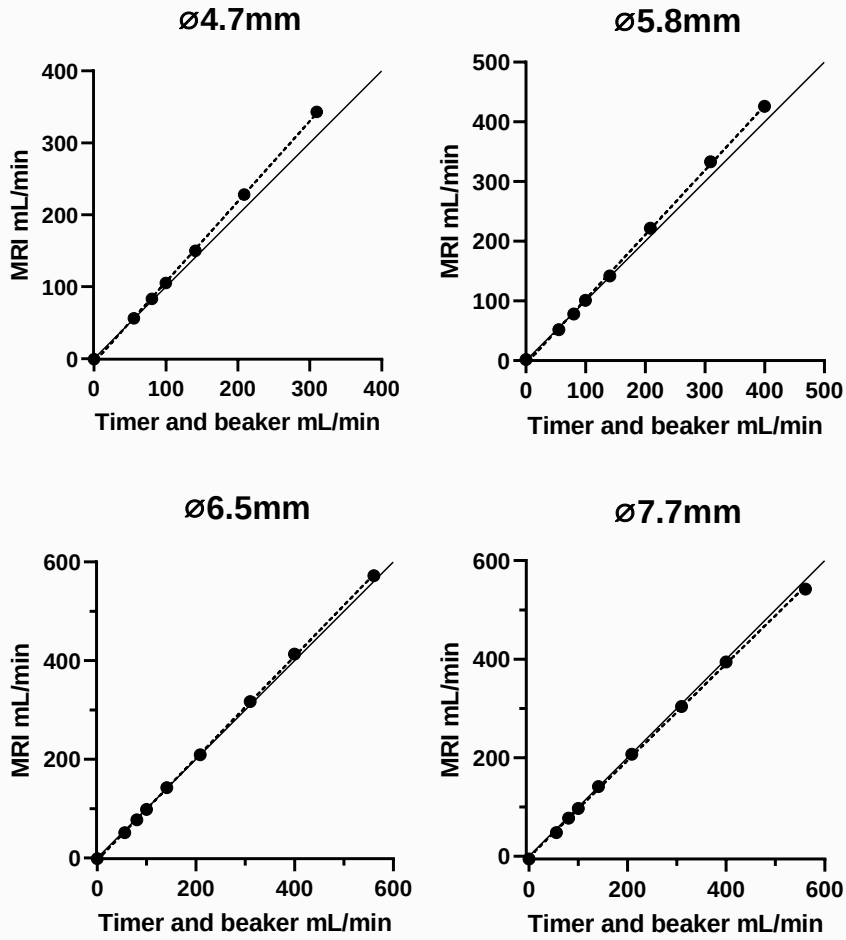

Figure 4.8: Magnetic resonance imaging (MRI) flow measurements vs. timer and beaker in a pulsatile flow phantom with 4.7mm, 5.8mm, 6.5mm, and 7.7mm diameter thin-walled plastic pipe. Solid line = line of identity. Dashed line = linear regression.

Chapter 5

Conclusions

The overall aim set out for this thesis was to determine how magnetic resonance imaging (MRI) can be utilized to determine myocardial perfusion (MP) abnormalities in patients with diseases that are known or suspected to have myocardial microvascular involvement.

Therefore, three studies were performed that investigated diseases that were known or suspected to have myocardial microvascular involvement (hypertrophic cardiomyopathy (HCM), systemic sclerosis (SSc) and microvascular angina (MVA)) with cardiac MRI. The fourth study of this thesis aimed to collect reference values for global MP from healthy volunteers and validate the MRI methods used to measure global MP in the different studies.

The main conclusions for each study (I - IV) are listed below.

I Study I found that young patients with HCM have lower global MP during adenosine stress than healthy volunteers. Patients with heritable risk of HCM but normal cardiac phenotype did not have lower global MP than healthy volunteers. The perfusion deficit was present even in the absence of diastolic dysfunction or left ventricular (LV) outflow tract obstruction. The observed coronary microvascular dysfunction (CMD) suggests that patients with HCM may suffer from cardiac microvascular disease.

II Study II reported that patients with SSc have lower global MP during adenosine stress compared to healthy volunteers. This finding suggest that patients with SSc suffer from cardiac microvascular disease. Future studies investigating the prognostic impact and effect of therapeutic regimes regarding global MP are motivated.

III Study III showed that patients with suspected MVA have lower global MP than healthy volunteers. Furthermore, there was a significant sex difference in global MP in healthy volunteers and patients with suspected MVA, which imposes a need for sex-specific normal limits for global MP assessment.

IV Study IV provided age and sex-specific values of global MP from MRI coronary sinus (CS) flow measurements. The study showed that global MP was lower in men than women, which needs to be recognized when interpreting a quantitative assessment of global MP. Furthermore, the CS flow measurement method was validated using a mechanical flow phantom.

Bibliography

[1] C. J. Wiggers. "Studies on the consecutive phases of the cardiac cycle". In: *American Journal of Physiology-Legacy Content* 56.3 (July 1921), pp. 415–438.

[2] W. B. Hood. "Regional venous drainage of the human heart." In: *British heart journal* 30.1 (Jan. 1968), pp. 105–9.

[3] R. F. Wilson, K. Wyche, B. V. Christensen, S. Zimmer, and D. D. Laxson. "Effects of adenosine on human coronary arterial circulation." In: *Circulation* 82.5 (Nov. 1990), pp. 1595–1606.

[4] M. J. Quiñones et al. "Coronary Vasomotor Abnormalities in Insulin-Resistant Individuals". In: *Annals of Internal Medicine* 140.9 (May 2004), p. 700.

[5] P.-J. Moro, A. Flavian, A. Jacquier, F. Kober, J. Quilici, B. Gaborit, J.-L. Bonnet, G. Moulin, P. J. Cozzone, and M. Bernard. "Gender differences in response to cold pressor test assessed with velocity-encoded cardiovascular magnetic resonance of the coronary sinus". In: *Journal of Cardiovascular Magnetic Resonance* 13.1 (2011), p. 54.

[6] S. Windecker et al. "2014 ESC/EACTS Guidelines on myocardial revascularization: The Task Force on Myocardial Revascularization of the European Society of Cardiology (ESC) and the European Association for Cardio-Thoracic Surgery (EACTS)". In: *European Heart Journal* 35.37 (Oct. 2014), pp. 2541–2619.

[7] O. R. Coelho-Filho, C. Rickers, R. Y. Kwong, and M. Jerosch-Herold. "MR myocardial perfusion imaging". In: *Radiology* 266.3 (Mar. 2013), pp. 701–715.

[8] I. Klem et al. "Improved Detection of Coronary Artery Disease by Stress Perfusion Cardiovascular Magnetic Resonance With the Use of Delayed Enhancement Infarction Imaging". In: *Journal of the American College of Cardiology* 47.8 (Apr. 2006), pp. 1630–1638.

[9] J. P. Greenwood et al. "Cardiovascular magnetic resonance and single-photon emission computed tomography for diagnosis of coronary heart disease (CE-MARC): a prospective trial". In: *The Lancet* 379.9814 (Feb. 2012), pp. 453–460.

[10] J. P. Greenwood et al. “Effect of Care Guided by Cardiovascular Magnetic Resonance, Myocardial Perfusion Scintigraphy, or NICE Guidelines on Subsequent Unnecessary Angiography Rates”. In: *JAMA* 316.10 (Sept. 2016), p. 1051.

[11] J. Schwitter et al. “MR-IMPACT: comparison of perfusion-cardiac magnetic resonance with single-photon emission computed tomography for the detection of coronary artery disease in a multicentre, multivendor, randomized trial”. In: *European Heart Journal* 29.4 (Feb. 2008), pp. 480–489.

[12] C. Jaarsma, T. Leiner, S. C. Bekkers, H. J. Crijns, J. E. Wildberger, E. Nagel, P. J. Nelemans, and S. Schalla. “Diagnostic Performance of Noninvasive Myocardial Perfusion Imaging Using Single-Photon Emission Computed Tomography, Cardiac Magnetic Resonance, and Positron Emission Tomography Imaging for the Detection of Obstructive Coronary Artery Disease”. In: *Journal of the American College of Cardiology* 59.19 (May 2012), pp. 1719–1728.

[13] H. Engblom et al. “Fully quantitative cardiovascular magnetic resonance myocardial perfusion ready for clinical use: a comparison between cardiovascular magnetic resonance imaging and positron emission tomography”. In: *Journal of Cardiovascular Magnetic Resonance* 19.1 (Dec. 2017), p. 78.

[14] P. Kellman, M. S. Hansen, S. Nielles-Vallespin, J. Nickander, R. Themudo, M. Ugander, and H. Xue. “Myocardial perfusion cardiovascular magnetic resonance: optimized dual sequence and reconstruction for quantification”. In: *Journal of Cardiovascular Magnetic Resonance* 19.1 (Dec. 2017), p. 43.

[15] F. E. Mordini, T. Haddad, L.-Y. Hsu, P. Kellman, T. B. Lowrey, A. H. Aletras, W. P. Bandettini, and A. E. Arai. “Diagnostic Accuracy of Stress Perfusion CMR in Comparison With Quantitative Coronary Angiography”. In: *JACC: Cardiovascular Imaging* 7.1 (Jan. 2014), pp. 14–22.

[16] H. Rahman, C. M. Scannell, O. M. Demir, M. Ryan, H. McConkey, H. Ellis, P. G. Masci, D. Perera, and A. Chiribiri. “High-Resolution Cardiac Magnetic Resonance Imaging Techniques for the Identification of Coronary Microvascular Dysfunction”. In: *JACC: Cardiovascular Imaging* (Nov. 2020).

[17] H. Arheden, M. Saeed, E. Törnqvist, G. Lund, M. F. Wendland, C. B. Higgins, and F. Ståhlberg. “Accuracy of segmented MR velocity mapping to measure small vessel pulsatile flow in a phantom simulating cardiac motion”. eng. In: *Journal of Magnetic Resonance Imaging* 13.5 (May 2001), pp. 722–728.

[18] J. W. Koskenvuo, J. J. Hartiala, J. Knuuti, H. Sakuma, J. O. Toikka, M. Komu, M. Saraste, and P. Niemi. “Assessing coronary sinus blood flow in patients with coronary artery disease: A comparison of phase-contrast MR imaging with positron emission tomography”. In: *American Journal of Roentgenology* 177.5 (Nov. 2001), pp. 1161–1166.

[19] J. W. Koskenvuo, H. Sakuma, P. Niemi, J. O. Toikka, J. Knuuti, H. Laine, M. Komu, M. Kormano, M. Saraste, and J. J. Hartiala. "Global myocardial blood flow and global flow reserve measurements by MRI and PET are comparable". In: *Journal of Magnetic Resonance Imaging* 13.3 (Mar. 2001), pp. 361–366.

[20] J. Schwitter et al. "Magnetic resonance-based assessment of global coronary flow and flow reserve and its relation to left ventricular functional parameters: A comparison with positron emission tomography". In: *Circulation* 101.23 (June 2000), pp. 2696–2702.

[21] A. C. Van Rossum, F. C. Visser, M. B. Hofman, M. A. Galjee, N. Westerhof, and J. Valk. "Global left ventricular perfusion: Noninvasive measurement with cine MR imaging and phase velocity mapping of coronary venous outflow". In: *Radiology*. Vol. 182. 3. Mar. 1992, pp. 685–691.

[22] G. K. Lund, M. F. Wendland, A. Shimakawa, H. Arheden, F. Ståhlberg, C. B. Higgins, and M. Saeed. "Coronary sinus flow measurement by means of velocity-encoded cine MR imaging: validation by using flow probes in dogs." In: *Radiology* 217.2 (Nov. 2000), pp. 487–493.

[23] Z. Shomanova, A. Florian, M. Bietenbeck, J. Waltenberger, U. Sechtem, and A. Yilmaz. "Diagnostic value of global myocardial perfusion reserve assessment based on coronary sinus flow measurements using cardiovascular magnetic resonance in addition to myocardial stress perfusion imaging". In: *European Heart Journal Cardiovascular Imaging* 18.8 (Aug. 2017), pp. 851–859.

[24] H. Rahman et al. "Coronary Microvascular Dysfunction Is Associated With Myocardial Ischemia and Abnormal Coronary Perfusion During Exercise". In: *Circulation* 140.22 (Nov. 2019), pp. 1805–1816.

[25] R. Indorkar, R. Y. Kwong, S. Romano, B. E. White, R. C. Chia, M. Trybula, K. Evans, C. Shenoy, and A. Farzaneh-Far. "Global Coronary Flow Reserve Measured During Stress Cardiac Magnetic Resonance Imaging Is an Independent Predictor of Adverse Cardiovascular Events". In: *JACC: Cardiovascular Imaging* 12.8 (Aug. 2018), pp. 1686–1695.

[26] G. D. Hutchins, M. Schwaiger, K. C. Rosenspire, J. Krivokapich, H. Schelbert, and D. E. Kuhl. "Noninvasive quantification of regional blood flow in the human heart using N-13 ammonia and dynamic positron emission tomographic imaging". In: *Journal of the American College of Cardiology* 15.5 (Apr. 1990), pp. 1032–1042.

[27] O. Muzik, R. S. Beanlands, G. D. Hutchins, T. J. Mangner, N. Nguyen, and M. Schwaiger. "Validation of nitrogen-13-ammonia tracer kinetic model for quantification of myocardial blood flow using PET". In: *Journal of Nuclear Medicine* 34.1 (1993), pp. 83–91.

[28] N. Ghosh, O. E. Rimoldi, R. S. B. Beanlands, and P. G. Camici. "Assessment of myocardial ischaemia and viability: role of positron emission tomography". In: *European Heart Journal* 31.24 (Dec. 2010), pp. 2984–2995.

[29] T. R. DeGrado et al. "Estimation of myocardial blood flow for longitudinal studies with13N-labeled ammonia and positron emission tomography". In: *Journal of Nuclear Cardiology* 3.6 PART I (Nov. 1996), pp. 494–507.

[30] R. T. George, M. Jerosch-Herold, C. Silva, K. Kitagawa, D. A. Bluemke, J. A. Lima, and A. C. Lardo. "Quantification of myocardial perfusion using dynamic 64-detector computed tomography". In: *Investigative Radiology* 42.12 (Dec. 2007), pp. 815–822.

[31] F. Bamberg et al. "Dynamic myocardial CT perfusion imaging for evaluation of myocardial ischemia as determined by MR imaging". In: *JACC: Cardiovascular Imaging* 7.3 (Mar. 2014), pp. 267–277.

[32] P. G. Camici, G. d'Amati, and O. Rimoldi. "Coronary microvascular dysfunction: mechanisms and functional assessment". In: *Nature Reviews Cardiology* 12.1 (Jan. 2015), pp. 48–62.

[33] C. Caiati, N. Zedda, C. Montaldo, R. Montisci, and S. Iliceto. "Contrast-enhanced transthoracic second harmonic echo doppler with adenosine". In: *Journal of the American College of Cardiology* 34.1 (July 1999), pp. 122–130.

[34] C. Caiati, C. Montaldo, N. Zedda, R. Montisci, M. Ruscazio, G. Lai, M. Cadeddu, L. Meloni, and S. Iliceto. "Validation of a new noninvasive method (contrast-enhanced transthoracic second harmonic echo Doppler) for the evaluation of coronary flow reserve: Comparison with intracoronary Doppler flow wire". In: *Journal of the American College of Cardiology* 34.4 (Oct. 1999), pp. 1193–1200.

[35] L. Cortigiani, F. Rigo, S. Gherardi, M. Galderisi, F. Bovenzi, E. Picano, and R. Sicari. "Prognostic Effect of Coronary Flow Reserve in Women Versus Men With Chest Pain Syndrome and Normal Dipyridamole Stress Echocardiography". In: *The American Journal of Cardiology* 106.12 (Dec. 2010), pp. 1703–1708.

[36] M. L. Marcus, D. B. Doty, L. F. Hiratzka, C. B. Wright, and C. L. Eastham. "Decreased coronary reserve: a mechanism for angina pectoris in patients with aortic stenosis and normal coronary arteries". In: *New England Journal of Medicine* 307.22 (Nov. 1982), pp. 1362–1366.

[37] J. W. Doucette, P. D. Corl, H. M. Payne, A. E. Flynn, M. Goto, M. Nassi, and J. Segal. "Validation of a Doppler guide wire for intravascular measurement of coronary artery flow velocity". In: *Circulation* 85.5 (May 1992), pp. 1899–1911.

[38] T. P. van de Hoef et al. “Impact of hyperaemic microvascular resistance on fractional flow reserve measurements in patients with stable coronary artery disease: insights from combined stenosis and microvascular resistance assessment”. In: *Heart* 100.12 (June 2014), pp. 951–959.

[39] T. P. van de Hoef et al. “Physiological Basis and Long-Term Clinical Outcome of Discordance Between Fractional Flow Reserve and Coronary Flow Velocity Reserve in Coronary Stenoses of Intermediate Severity”. In: *Circulation: Cardiovascular Interventions* 7.3 (June 2014), pp. 301–311.

[40] F. Crea, P. G. Camici, and C. N. Bairey Merz. “Coronary microvascular dysfunction: an update”. In: *European Heart Journal* 35.17 (May 2014), pp. 1101–1111.

[41] J. L. Zamorano et al. “2014 ESC guidelines on diagnosis and management of hypertrophic cardiomyopathy: The task force for the diagnosis and management of hypertrophic cardiomyopathy of the European Society of Cardiology (ESC)”. In: *European Heart Journal* 35.39 (Oct. 2014), pp. 2733–2779.

[42] B. J. Maron, J. M. Gardin, J. M. Flack, S. S. Gidding, T. T. Kurosaki, and D. E. Bild. “Prevalence of hypertrophic cardiomyopathy in a general population of young adults: Echocardiographic analysis of 4111 subjects in the CARDIA study”. In: *Circulation* 92.4 (Aug. 1995), pp. 785–789.

[43] D. Corrado, C. Basso, M. Schiavon, and G. Thiene. “Screening for Hypertrophic Cardiomyopathy in Young Athletes”. In: *New England Journal of Medicine* 339.6 (Aug. 1998), pp. 364–369.

[44] C. Semsarian, J. Ingles, M. S. Maron, and B. J. Maron. “New perspectives on the prevalence of hypertrophic cardiomyopathy”. In: *Journal of the American College of Cardiology* 65.12 (Mar. 2015), pp. 1249–1254.

[45] L. R. Lopes, A. Zekavati, P. Syrris, M. Hubank, C. Giambartolomei, C. Dalageorgou, S. Jenkins, W. McKenna, V. Plagnol, and P. M. Elliott. “Genetic complexity in hypertrophic cardiomyopathy revealed by high-throughput sequencing”. In: *Journal of Medical Genetics* 50.4 (Apr. 2013), pp. 228–239.

[46] H. Morita, H. L. Rehm, A. Menesses, B. McDonough, A. E. Roberts, R. Kucherlapati, J. A. Towbin, J. Seidman, and C. E. Seidman. “Shared Genetic Causes of Cardiac Hypertrophy in Children and Adults”. In: *New England Journal of Medicine* 358.18 (May 2008), pp. 1899–1908.

[47] I. Olivotto et al. “Myofilament protein gene mutation screening and outcome of patients with hypertrophic cardiomyopathy”. In: *Mayo Clinic Proceedings* 83.6 (June 2008), pp. 630–638.

[48] I. Ostman-Smith, G. Wettrell, B. Keeton, D. Holmgren, U. Ergander, S. Gould, C. Bowker, and M. Verdicchio. "Age- and gender-specific mortality rates in childhood hypertrophic cardiomyopathy". eng. In: *European heart journal* 29.9 (May 2008), pp. 1160–1167.

[49] B. J. Maron. "Sudden Death in Young Athletes". In: *New England Journal of Medicine* 349.11 (Sept. 2003), pp. 1064–1075.

[50] P. Richard et al. "Hypertrophic cardiomyopathy: Distribution of disease genes, spectrum of mutations, and implications for a molecular diagnosis strategy". In: *Circulation* 107.17 (May 2003), pp. 2227–2232.

[51] F. S. Korte, K. S. McDonald, S. P. Harris, and R. L. Moss. "Loaded Shortening, Power Output, and Rate of Force Redevelopment Are Increased With Knockout of Cardiac Myosin Binding Protein-C". In: *Circulation Research* 93.8 (Oct. 2003), pp. 752–758.

[52] S. P. Harris, C. R. Bartley, T. A. Hacker, K. S. McDonald, P. S. Douglas, M. L. Greaser, P. A. Powers, and R. L. Moss. "Hypertrophic cardiomyopathy in cardiac myosin binding protein-C knockout mice". In: *Circulation Research* 90.5 (Mar. 2002), pp. 594–601.

[53] B. J. Maron, J. K. Wolfson, S. E. Epstein, and W. C. Roberts. "Intramural ("small vessel") coronary artery disease in hypertrophic cardiomyopathy". In: *Journal of the American College of Cardiology* 8.3 (Sept. 1986), pp. 545–557.

[54] P. Camici, G. Chiriatti, R. Lorenzoni, R. C. Bellina, R. Gistri, G. Italiani, O. Parodi, P. A. Salvadori, N. Nista, and L. Papi. "Coronary vasodilation is impaired in both hypertrophied and nonhypertrophied myocardium of patients with hypertrophic cardiomyopathy: a study with nitrogen-13 ammonia and positron emission tomography". In: *Journal of the American College of Cardiology* 17.4 (Mar. 1991), pp. 879–886.

[55] L. Choudhury, P. Elliott, O. Rimoldi, M. Ryan, A. A. Lammertsma, H. Boyd, W. J. McKenna, and P. G. Camici. "Transmural myocardial blood flow distribution in hypertrophic cardiomyopathy and effect of treatment". eng. In: *Basic research in cardiology* 94.1 (Feb. 1999), pp. 49–59.

[56] F. Cecchi, I. Olivotto, R. Gistri, R. Lorenzoni, G. Chiriatti, and P. G. Camici. "Coronary Microvascular Dysfunction and Prognosis in Hypertrophic Cardiomyopathy". In: *New England Journal of Medicine* 349.11 (Sept. 2003), pp. 1027–1035.

[57] T. F. Ismail et al. "Coronary microvascular ischemia in hypertrophic cardiomyopathy - a pixel-wise quantitative cardiovascular magnetic resonance perfusion study." In: *Journal of cardiovascular magnetic resonance : official journal of the Society for Cardiovascular Magnetic Resonance* 16.1 (Aug. 2014), p. 49.

[58] O. Kowal-Bielecka et al. “Update of EULAR recommendations for the treatment of systemic sclerosis”. In: *Annals of the Rheumatic Diseases* 76.8 (Aug. 2017), pp. 1327–1339.

[59] M. Nikpour, W. M. Stevens, A. L. Herrick, and S. M. Proudman. “Epidemiology of systemic sclerosis”. In: *Best Practice & Research Clinical Rheumatology* 24.6 (Dec. 2010), pp. 857–869.

[60] F. A. Wollheim. “Classification of systemic sclerosis. Visions and reality”. In: *Rheumatology* 44.10 (Oct. 2005), pp. 1212–1216.

[61] K. Kawaji et al. “Automated segmentation of routine clinical cardiac magnetic resonance imaging for assessment of left ventricular diastolic dysfunction”. In: *Circulation. Cardiovascular imaging* 2.6 (Nov. 2009), pp. 476–484.

[62] L. Czirják, G. Kumánovics, C. Varjú, Z. Nagy, A. Pákozdi, Z. Szekanecz, and G. Szucs. “Survival and causes of death in 366 Hungarian patients with systemic sclerosis.” In: *Annals of the rheumatic diseases* 67.1 (Jan. 2008), pp. 59–63.

[63] K. Au, M. K. Singh, V. Bodukam, S. Bae, P. Maranian, R. Ogawa, B. Spiegel, M. McMahon, B. Hahn, and D. Khanna. “Atherosclerosis in systemic sclerosis: A systematic review and meta-analysis”. In: *Arthritis & Rheumatism* 63.7 (July 2011), pp. 2078–2090.

[64] W. A. D’Angelo, J. F. Fries, A. T. Masi., and L. E. Shulman. “Pathologic observations in systemic sclerosis (scleroderma)”. In: *The American Journal of Medicine* 46.3 (Mar. 1969), pp. 428–440.

[65] A. Kahan, A. Nitenberg, J. M. Foult, B. Amor, C. J. Menkes, J. Y. Devaux, F. Blanchet, J. Perennec, G. Lutfalla, and J. C. Roucayrol. “Decreased coronary reserve in primary scleroderma myocardial disease”. en. In: *Arthritis and rheumatism* 28.6 (June 1985), pp. 637–46.

[66] Y. Allanore, C. Meune, and A. Kahan. “Systemic sclerosis and cardiac dysfunction: evolving concepts and diagnostic methodologies.” In: *Current opinion in rheumatology* 20 (2008), pp. 697–702.

[67] V. Kunadian et al. “An EAPCI Expert Consensus Document on Ischaemia with Non-Obstructive Coronary Arteries in Collaboration with European Society of Cardiology Working Group on Coronary Pathophysiology & Microcirculation Endorsed by Coronary Vasomotor Disorders International”. In: *EuroIntervention* 16.13 (Jan. 2021), pp. 1049–1069.

[68] H. Suzuki. “Different definition of microvascular angina”. In: *European Journal of Clinical Investigation* 45.12 (Dec. 2015), pp. 1360–1366.

[69] L. Jespersen et al. “Stable angina pectoris with no obstructive coronary artery disease is associated with increased risks of major adverse cardiovascular events”. In: *European Heart Journal* 33.6 (Sept. 2012), pp. 734–744.

[70] T. M. Maddox et al. “Nonobstructive Coronary Artery Disease and Risk of Myocardial Infarction”. In: *JAMA - Journal of the American Medical Association* 312.17 (Nov. 2014), pp. 1754–1763.

[71] J. Knuuti et al. “2019 ESC Guidelines for the diagnosis and management of chronic coronary syndromes”. In: *European Heart Journal* 41.3 (Jan. 2020), pp. 407–477.

[72] J. Escaned et al. “Assessment of microcirculatory remodeling with intracoronary flow velocity and pressure measurements: Validation with endomyocardial sampling in cardiac allografts”. In: *Circulation* 120.16 (Oct. 2009), pp. 1561–1568.

[73] R. Herscovici, T. Sedlak, J. Wei, C. J. Pepine, E. Handberg, and C. N. Bairey Merz. “Ischemia and No Obstructive Coronary Artery Disease (INOCA): What Is the Risk?” In: *Journal of the American Heart Association* 7.17 (Sept. 2018).

[74] J. C. Kaski, P. Collins, P. Nihoyannopoulos, A. Maseri, P. A. Poole-Wilson, and G. M. Rosano. “Cardiac syndrome X: Clinical characteristics and left ventricular function: Long-term follow-up study”. In: *Journal of the American College of Cardiology* 25.4 (Mar. 1995), pp. 807–814.

[75] D. Opherk, G. Mall, H. Zebe, F. Schwarz, E. Weihe, J. Manthey, and W. Kübler. “Reduction of coronary reserve: a mechanism for angina pectoris in patients with arterial hypertension and normal coronary arteries.” In: *Circulation* 69.1 (Jan. 1984), pp. 1–7.

[76] A. Kibel, K. Selthofer-Relatic, I. Drenjancevic, T. Bacun, I. Bosnjak, D. Kibel, and M. Gros. “Coronary microvascular dysfunction in diabetes mellitus.” In: *The Journal of international medical research* 45.6 (Dec. 2017), pp. 1901–1929.

[77] S. E. Reis, R. Holubkov, A. J. C. Smith, S. F. Kelsey, B. L. Sharaf, N. Reichek, W. J. Rogers, C. N. B. Merz, G. Sopko, and C. J. Pepine. “Coronary microvascular dysfunction is highly prevalent in women with chest pain in the absence of coronary artery disease: Results from the NHLBI WISE study”. In: *American Heart Journal* 141.5 (May 2001), pp. 735–741.

[78] K. Bove, M. Nilsson, L. Pedersen, N. Mikkelsen, H. Suhrs, A. Astrup, and E. Prescott. “Effect of weight loss, exercise and risk factor control in microvascular angina. A randomized controlled pilot trial”. In: *European Heart Journal* 41.Supplement_2 (Nov. 2020).

[79] V. L. Murthy et al. “Improved Cardiac Risk Assessment With Noninvasive Measures of Coronary Flow Reserve”. In: *Circulation* 124.20 (Nov. 2011), pp. 2215–2224.

[80] L.-M. Gan, S. Svedlund, A. Wittfeldt, C. Eklund, S. Gao, G. Matejka, A. Jeppsson, P. Albertsson, E. Omerovic, and A. Lerman. "Incremental Value of Transthoracic Doppler Echocardiography□Assessed Coronary Flow Reserve in Patients With Suspected Myocardial Ischemia Undergoing Myocardial Perfusion Scintigraphy". In: *Journal of the American Heart Association* 6.4 (Apr. 2017).

[81] K. D. Knott et al. "The Prognostic Significance of Quantitative Myocardial Perfusion: An Artificial Intelligence-Based Approach Using Perfusion Mapping". In: *Circulation* (Feb. 2020), pp. 1282–1291.

[82] V. R. Taqueti et al. "Coronary microvascular dysfunction and future risk of heart failure with preserved ejection fraction". In: *European Heart Journal* 39.10 (Mar. 2018), pp. 840–849.

[83] Y. Kanaji et al. "Prognostic value of coronary flow capacity assessed by coronary sinus flow obtained by phase contrast cine-magnetic resonance imaging in patients with acute coronary syndrome". In: *European Heart Journal* 41.Supplement_2 (Nov. 2020).

[84] I. I. Rabi, J. R. Zacharias, S. Millman, and P. Kusch. "A New Method of Measuring Nuclear Magnetic Moment". In: *Physical Review* 53.4 (Feb. 1938), pp. 318–318.

[85] R. R. Edelman. "The History of MR Imaging as Seen through the Pages of Radiology". In: *Radiology* 273.2S (Nov. 2014), S181–S200.

[86] R. Damadian. "Tumor Detection by Nuclear Magnetic Resonance". In: *Science* 171.3976 (Mar. 1971), pp. 1151–1153.

[87] P. C. Lauterbur. "Image formation by induced local interactions: Examples employing nuclear magnetic resonance". In: *Nature* 242.5394 (1973), pp. 190–191.

[88] P. Mansfield, A. A. Maudsley, and T. Bains. "Fast scan proton density imaging by NMR". In: *Journal of Physics E: Scientific Instruments* 9.4 (1976), pp. 271–278.

[89] P. Mansfield and A. A. Maudsley. "Medical imaging by NMR". In: *British Journal of Radiology* 50.591 (1977), pp. 188–194.

[90] J. R. Mallard. "The contribution of medical physicists and doctors in Aberdeen to the evolution of modern medical imaging - SPECT, PET and MRI, 1965-1992". In: *Scottish Medical Journal* 51.2 (May 2006), pp. 44–48.

[91] D. W. McRobbie, E. A. Moore, and M. J. Graves. *MRI from Picture to Proton*. Cambridge: Cambridge University Press, 2017.

[92] X. He et al. "First in-vivo human imaging at 10.5T: Imaging the body at 447 MHz". In: *Magnetic Resonance in Medicine* 84.1 (July 2020), pp. 289–303.

[93] D. G. Gadian, D. I. Hoult, G. K. Radda, P. J. Seeley, B. Chance, and C. Barlow. "Phosphorus nuclear magnetic resonance studies on normoxic and ischemic cardiac tissue". In: *Proceedings of the National Academy of Sciences of the United States of America* 73.12 (Dec. 1976), pp. 4446–4448.

[94] M. R. Goldman, T. J. Brady, I. L. Pykett, C. T. Burt, F. S. Buonanno, J. P. Kistler, J. H. Newhouse, W. S. Hinshaw, and G. M. Pohost. "Quantification of experimental myocardial infarction using nuclear magnetic resonance imaging and paramagnetic ion contrast enhancement in excised canine hearts". In: *Circulation* 66.5 I (1982), pp. 1012–1016.

[95] C. B. Higgins, R. Herfkens, M. J. Lipton, R. Sievers, P. Sheldon, L. Kaufman, and L. E. Crooks. "Nuclear magnetic resonance imaging of acute myocardial infarction in dogs: Alterations in magnetic relaxation times". In: *The American Journal of Cardiology* 52.1 (July 1983), pp. 184–188.

[96] D. J. Atkinson, D. Burstein, and R. R. Edelman. "First-pass cardiac perfusion: Evaluation with ultrafast MR imaging". In: *Radiology* 174.3 (Mar. 1990), pp. 757–762.

[97] D. J. Bryant, J. A. Payne, D. N. Firmin, and D. B. Longmore. "Measurement of flow with nmr imaging using a gradient pulse and phase difference technique". In: *Journal of Computer Assisted Tomography* 8.4 (1984), pp. 588–593.

[98] M. Carlsson, J. Jögi, K. M. Bloch, B. Hedén, U. Ekelund, F. Ståhlberg, and H. Arheden. "Submaximal adenosine-induced coronary hyperaemia with 12 h caffeine abstinence: implications for clinical adenosine perfusion imaging tests". In: *Clinical Physiology and Functional Imaging* 35.1 (2015), pp. 49–56.

[99] F. van den Hoogen et al. "2013 classification criteria for systemic sclerosis: an American college of rheumatology/European league against rheumatism collaborative initiative". en. In: *Annals of the Rheumatic Diseases* 72.11 (Nov. 2013), pp. 1747–1755.

[100] E. Heiberg, J. Sjögren, M. Ugander, M. Carlsson, H. Engblom, and H. Arheden. "Design and validation of Segment - freely available software for cardiovascular image analysis". In: *BMC Medical Imaging* 10.1 (2010), p. 1.

[101] K. M. Bloch, M. Carlsson, H. Arheden, and F. Ståhlberg. "Quantifying coronary sinus flow and global LV perfusion at 3T". In: *BMC Medical Imaging* 9.1 (Dec. 2009), p. 9.

[102] F. L. Gobel, L. A. Norstrom, R. R. Nelson, C. R. Jorgensen, and Y. Wang. "The rate-pressure product as an index of myocardial oxygen consumption during exercise in patients with angina pectoris." In: *Circulation* 57.3 (Mar. 1978).

[103] E. Heiberg, M. Ugander, H. Engblom, M. Götberg, G. K. Olivecrona, D. Erlinge, and H. Arheden. "Automated quantification of myocardial infarction from MR images by accounting for partial volume effects: animal, phantom, and human study". In: *Radiology* 246.2 (Feb. 2008), pp. 581–588.

[104] H. Engblom et al. "A new automatic algorithm for quantification of myocardial infarction imaged by late gadolinium enhancement cardiovascular magnetic resonance: experimental validation and comparison to expert delineations in multi-center, multi-vendor patient data". In: *Journal of Cardiovascular Magnetic Resonance* 18.1 (2016), p. 27.

[105] L. Jorfeldt and O. Pahlm, eds. *Kliniska arbetsprov : metoder för diagnos och prognos*. 1st ed. Lund: Studentlitteratur AB, 2013.

[106] Y. Sugishita, M. Matsuda, K. Iida, J. Koshinaga, and M. Ueno. "Sudden cardiac death at exertion." In: *Japanese Circulation Journal* 47.5 (1983), pp. 562–572.

[107] B. J. Maron. "Sudden Death in Young Competitive Athletes". In: *JAMA* 276.3 (July 1996), p. 199.

[108] N. Kawada, H. Sakuma, T. Yamakado, K. Takeda, N. Isaka, T. Nakano, and C. B. Higgins. "Hypertrophic cardiomyopathy: MR measurement of coronary blood flow and vasodilator flow reserve in patients and healthy subjects". In: *Radiology* 211.1 (Apr. 1999), pp. 129–135.

[109] S. E. Petersen, M. Jerosch-Herold, L. E. Hudsmith, M. D. Robson, J. M. Francis, H. A. Doll, J. B. Selvanayagam, S. Neubauer, and H. Watkins. "Evidence for microvascular dysfunction in hypertrophic cardiomyopathy: New insights from multiparametric magnetic resonance imaging". In: *Circulation* 115.18 (Apr. 2007), pp. 2418–2425.

[110] S. F. Nagueh, C. P. Appleton, T. C. Gillebert, P. N. Marino, J. K. Oh, O. A. Smiseth, A. D. Waggoner, F. A. Flachskampf, P. A. Pellikka, and A. Evangelisa. "Recommendations for the Evaluation of Left Ventricular Diastolic Function by Echocardiography". In: *European Journal of Echocardiography* 10.2 (Aug. 2008), pp. 165–193.

[111] L. Galiuto and European Association of Echocardiography. *The EAE Textbook of Echocardiography*. English. Ed. by L. Galiuto, L. Badano, K. Fox, R. Sicari, and J. L. Zamorano. Vol. 1. Oxford: Oxford University Press, Mar. 2011.

[112] J. W. McNamara, A. Li, S. Lal, J. M. Bos, S. P. Harris, J. Van Der Velden, M. J. Ackerman, R. Cooke, and C. G. Dos Remedios. "MYBPC3 mutations are associated with a reduced super-relaxed state in patients with hypertrophic cardiomyopathy". In: *PLoS ONE* 12.6 (June 2017), e0180064.

[113] B. P. Kimball, V. LiPreti, S. Bui, and E. Wigle. "Comparison of proximal left anterior descending and circumflex coronary artery dimensions in aortic valve stenosis and hypertrophic cardiomyopathy". In: *The American Journal of Cardiology* 65.11 (Mar. 1990), pp. 767–771.

[114] M. R. Akram, C. E. Handler, M. Williams, M. T. Carulli, M. Andron, C. M. Black, C. P. Denton, and J. G. Coghlan. "Angiographically proven coronary artery disease in scleroderma". en. In: *Rheumatology* 45.11 (Aug. 2006), pp. 1395–1398.

[115] V. D. Steen, W. P. Follansbee, C. G. Conte, and T. a. Medsger. "Thallium perfusion defects predict subsequent cardiac dysfunction in patients with systemic sclerosis." In: *Arthritis and rheumatism* 39.4 (1996), pp. 677–681.

[116] R. Montisci, a. Vacca, P. Garau, P. Colonna, M. Ruscazio, G. Passiu, S. Iliceto, and a. Mathieu. "Detection of early impairment of coronary flow reserve in patients with systemic sclerosis." In: *Annals of the rheumatic diseases* 62 (2003), pp. 890–893.

[117] A. Gigante et al. "Role of autonomic dysfunction in the regulation of myocardial blood flow in systemic sclerosis evaluated by cardiac magnetic resonance". In: *International Journal of Rheumatic Diseases* 22.6 (Apr. 2019), pp. 1756–185.

[118] S. Sato Saigusa et al. "Vasculopathy in Systemic Sclerosis Endothelial Cells, Contributing to the Development of Fibrosis and Fli1 Deficiency Induces CXCL6 Expression in Dermal Fibroblasts and Fli1 Deficiency Induces CXCL6 Expression in Dermal Fibroblasts and Endothelial Cells, " in: *The Journal of Rheumatology* 44.8 (2017), pp. 1198–1205.

[119] Y. Asano. "Epigenetic suppression of Fli1, a potential predisposing factor in the pathogenesis of systemic sclerosis". In: *International Journal of Biochemistry and Cell Biology* (2015).

[120] J. R. Panting, P. D. Gatehouse, G.-Z. Yang, F. Grothues, D. N. Firmin, P. Collins, D. J. Pennell, R. B. Hospital, and N. Heart. "Abnormal Subendocardial Perfusion in Cardiac Syndrome X Detected by Cardiovascular Magnetic Resonance Imaging". eng. In: *The New England journal of medicine* 346.25 (June 2002), pp. 1948–1953.

[121] P. Chareonthaitawee, P. A. Kaufmann, O. Rimoldi, and P. G. Camici. "Heterogeneity of resting and hyperemic myocardial blood flow in healthy humans". In: *Cardiovascular Research* 50.1 (Apr. 2001), pp. 151–161.

[122] H. J. Verberne et al. "EANM procedural guidelines for radionuclide myocardial perfusion imaging with SPECT and SPECT/CT: 2015 revision". In: *European Journal of Nuclear Medicine and Molecular Imaging* 42.12 (2015), pp. 1929–1940.

[123] N. D. Mygind et al. “Coronary microvascular function and cardiovascular risk factors in women with angina pectoris and no obstructive coronary artery disease: The iPOWER study”. In: *Journal of the American Heart Association* 5.3 (Mar. 2015).

[124] C. Gebhard et al. “Sex differences in the long-term prognostic value of 13N-ammonia myocardial perfusion positron emission tomography”. In: *European Journal of Nuclear Medicine and Molecular Imaging* 45.11 (Oct. 2018), pp. 1964–1974.

[125] V. L. Murthy et al. “Effects of sex on coronary microvascular dysfunction and cardiac outcomes”. In: *Circulation* 129.24 (June 2014), pp. 2518–2527.

[126] C. J. Pepine, R. D. Anderson, B. L. Sharaf, S. E. Reis, K. M. Smith, E. M. Handberg, B. D. Johnson, G. Sopko, and C. N. Bairey Merz. “Coronary Microvascular Reactivity to Adenosine Predicts Adverse Outcome in Women Evaluated for Suspected Ischemia”. In: *Journal of the American College of Cardiology* 55.25 (June 2010), pp. 2825–2832.

[127] J. Schroder, M. M. Michelsen, N. D. Mygind, H. E. Suhrs, K. B. Bove, D. F. Bechsgaard, A. Aziz, I. Gustafsson, J. Kastrup, and E. Prescott. “Coronary flow velocity reserve predicts adverse prognosis in women with angina and no obstructive coronary artery disease: results from the iPOWER study”. In: *European Heart Journal* 42.3 (Jan. 2021), pp. 228–239.

[128] C. Bairey Merz, S. F. Kelsey, C. J. Pepine, N. Reichek, S. E. Reis, W. J. Rogers, B. L. Sharaf, and G. Sopko. “The Women’s Ischemia Syndrome Evaluation (WISE) Study: protocol design, methodology and feasibility report”. In: *Journal of the American College of Cardiology* 33.6 (May 1999), pp. 1453–1461.

[129] L. E. Thomson et al. “Cardiac Magnetic Resonance Myocardial Perfusion Reserve Index Is Reduced in Women With Coronary Microvascular Dysfunction”. In: *Circulation: Cardiovascular Imaging* 8.4 (Apr. 2015), pp. 1–9.

[130] A. C. van Rossum, F. C. Visser, M. B. Hofman, M. A. Galjee, N. Westerhof, and J. Valk. “Global left ventricular perfusion: noninvasive measurement with cine MR imaging and phase velocity mapping of coronary venous outflow.” In: *Radiology* 182.3 (Mar. 1992), pp. 685–91.

[131] D. L. Johnston, D. O. Hodge, M. R. Hopfenspirger, and R. J. Gibbons. “Clinical Determinants of Hemodynamic and Symptomatic Responses in 2,000 Patients During Adenosine Scintigraphy”. In: *Mayo Clinic Proceedings* 73.4 (Apr. 1998), pp. 314–320.

[132] J. Czernin, P. Müller, S. Chan, R. C. Brunken, G. Porenta, J. Krivokapich, K. Chen, A. Chan, M. E. Phelps, and H. R. Schelbert. “Influence of age and hemodynamics on myocardial blood flow and flow reserve”. In: *Circulation* 88.1 (July 1993), pp. 62–69.

[133] N. G. Uren, P. G. Camici, J. a. Melin, a. Bol, B. de Bruyne, J. Radvan, I. Olivotto, S. D. Rosen, M. Impallomeni, and W. Wijns. "Effect of aging on myocardial perfusion reserve." In: *Journal of nuclear medicine : official publication, Society of Nuclear Medicine* 36.13 (1995), pp. 2032–2036.

[134] J. Nickander, R. Themudo, A. Sigfridsson, H. Xue, P. Kellman, and M. Ugander. "Females have higher myocardial perfusion, blood volume and extracellular volume compared to males – an adenosine stress cardiovascular magnetic resonance study". In: *Scientific Reports* 10.1 (Dec. 2020), p. 10380.

[135] S. Sdringola, N. P. Johnson, R. L. Kirkeeide, E. Cid, and K. L. Gould. "Impact of unexpected factors on quantitative myocardial perfusion and coronary flow reserve in young, asymptomatic volunteers". In: *JACC: Cardiovascular Imaging* 4.4 (2011), pp. 402–412.

[136] J. D. Rossen, J. E. Quillen, J. G. Lopez, R. G. Stenberg, C. L. Talman, and M. D. Winniford. "Comparison of coronary vasodilation with intravenous dipyridamole and adenosine". In: *Journal of the American College of Cardiology* 18.2 (Aug. 1991), pp. 485–491.

[137] P. A. Kaufmann, T. Gnecchi-Ruscone, K. P. Schäfers, T. F. Lüscher, and P. G. Camici. "Low density lipoprotein cholesterol and coronary microvascular dysfunction in hypercholesterolemia". In: *Journal of the American College of Cardiology* 36.1 (July 2000), pp. 103–109.